Impact of a Near-Surface Plasma Region on the Bow Shock Wave and Aerodynamic Characteristics of a High-Speed Model in Xenon

Olga A. Azarova *, Tatiana A. Lapushkina, Oleg V. Kravchenko

Posted Date: 16 October 2024

doi: 10.20944/preprints202410.1285.v1

Keywords:

supersonic flow; bow shock wave control; near-surface energy deposition; glow gas discharge; discharge plasma parameters; drag force control

Article

Impact of a Near-Surface Plasma Region on the Bow Shock Wave and Aerodynamic Characteristics of a High-Speed Model in Xenon

Olga A. Azarova [1,*], Tatiana A. Lapushkina [1,2] and Oleg V. Kravchenko [1]

[1] Federal Research Center "Computer Science and Control" of the Russian Academy of Sciences, Russia, Moscow, 119333, Vavilova str. 44

[2] Ioffe Institute, Russia, St Petersburg, 194021, Politekhnicheskaya str. 26

* Correspondence: olgazarov@gmail.com

Abstract: The main objective of the present study is to demonstrate the possibility of actively influencing the position of the bow shock wave and the main parameters of supersonic flow over a blunt body by organizing a gas discharge near the front surface, in the region between the body and the bow shock wave. The research is carried out using both experimental and numerical methods. The working gas was xenon. It is shown that the steady bow shock wave stand-off distance along with the current and power of the discharge, is associated with the change in the adiabatic index of the plasma created by the discharge, which, in turn, is determined by the plasma parameters, such as the degrees of nonequilibrium and the degree of ionization. It is shown that the adiabatic index with the power supplied to the impact zone in the range of 30-120 kW can both increase and decrease in the range of 1.25-1.288. The study of the discharge created plasma zone was conducted and the correspondence between the discharge current and power, and the average parameters in the plasma zone created by the discharge is presented. A good agreement between the numerical and experimental data was shown. The results may be useful in developing control systems for high-speed civil aircrafts.

Keywords: supersonic flow; bow shock wave control; near-surface energy deposition; glow gas discharge; discharge plasma parameters; drag force control

1. Introduction

The issue of controlling the bow shock wave represents a significant aspect within the research of supersonic/hypersonic flow control, as the standoff distance of the bow shock directly affects upon the aerodynamic characteristics of a streamlined body (see [1] by D. Knight). Surveys of research pertaining to energy deposition for flow/flight control were presented by D. Knight [2], M. Ahmed and N. Qin [3], and S. Rashid et al. [4]. S. Leonov et al. provided an overview of researches devoted to the interaction of airflow with a range of surface-based gas discharges and discussed experiments concerning the control of supersonic flow structures through near-surface discharges [5,6]. I. Znamenskaya in the review [7], discussed different visualization techniques such as refraction-based methods, electroluminescence, particle image velocimetry, and surface visualization techniques.

Theoretical considerations concerning the impact of energy deposition in a freestream flow on the bow shock and the parameters of an AD body are discussed by P. Georgievsky and V. Levin in [8], V. Artem'ev et al. in [9], and D. Riggins et al. in [10]. Experimental investigations demonstrated the possibility of a significant influence on a supersonic flow using a variety of methods, including MW impulse (Y. Kolesnichenko et al. [11]), laser (P. Tretyakov et al. [12]), electrical discharge (V. Bityurin et al. [13,14], N. Benard and E. Moreau [15]), and MHD effects (T. Lapushkina and A. Erofeev [16]).

The dynamics of xenon plasma flow within a supersonic diffuser, influenced by external electric and magnetic fields, were investigated by T. Lapushkina et al. in [17]. Experimental results showed

 doi:10.20944/preprints202410.1285.v1

that during heating of noble gas plasma in nonequilibrium conditions, the energy level, which determines the ionization rate, shifts towards a lower energy, which allows ionization of the expanding flow for subsequent MHD experiments. In [18,19], S. Bobashev et al. has revealed that external electric and magnetic fields exert a significant influence on the structural transformations occurring in the supersonic flow of weakly ionized xenon and MHD effects have a significant influence on the magnitude of the heat flux directed to the plate surface in the flow. The characteristics of the hydrodynamic phenomenon arising from high-speed flow over a surface of a blunt fin were considered by X. Zhao in [20]. It was shown that the generation of the shock wave by the rib leads to early separation of the boundary layer in front of the rib, and the increase in pressure in the head part of the shock wave generated by the rib led to the detachment of the boundary layer, resulting in the formation of a region of separated flow. A substantial research has been conducted to ascertain the influence of diverse energy sources, distinguished by their geometric configuration and placement, on the bow shock wave. The impact of an arc gas discharge on the location of an oblique shock wave and the distribution of pressure within the flow was attributed to thermal effects and was modeled by H. Yan et al. in [21]. Also, B. Tang et al. investigated the regulation of a cylindrical detached bow shock wave and the modification of the shock wave angle through the high-energy stimulation of surface arc discharge plasma in [22]. These effects were attributed to the heating of the gas, which subsequently leads to the deformation of the bow shock wave.

It is notable that among the studies on the bow shock wave control by energy deposition, a comparatively limited number of investigations were focused on the impact of plasma region parameters, such as the degree of ionization and nonequilibrium. Nevertheless, the introduction of charged particles, including electrons and ions, into the surrounding gas flow of an AD alongside the thermodynamic nonequilibrium, characterized by a predominance of electron temperature over gas temperature, results in an additional displacement of the bow shock wave compared with the consequence of purely thermal shifts. In [23], Azarova et al. compared experimental data on the thermal nonequilibrium flow of an AD body with the results of modelling assuming a thermal mechanism of the discharge action. The experiments demonstrated the influence of plasma on the dynamics of the bow shock wave, which is associated with nonequilibrium ionization in the flow. The dependences of the adiabatic index (isentropic exponent) and specific heat capacities as functions of the degree of ionization and the degree of nonequilibrium for monatomic plasma in the absence of local thermodynamic equilibrium are presented by K. Burm et al. in [24].

In [25], V. Lago et al. examined the impact of a gas discharge near the surface of a streamlined body on the bow shock. The study involves the use of electrogasdynamic and magnetohydrodynamic methods to adjust the position of the bow shock wave. Experimental results for a Mach 2 flow showed that increasing the power of the gas discharge near the body surface leads to an increase in the bow shock stand-off distance. Numerical simulations suggested that this shift in the bow shock position is influenced by both thermal effects and specific plasma properties like thermal nonequilibrium and ionization. The control of supersonic flow at a Mach number of 4 past an AD body examined through the energy supply to its surface via organization of a gas discharge across the entire cylindrical frontal surface is described by O. Azarova et al. in [26]. This study demonstrated the potential to influence both the position of the steady bow shock wave and the aerodynamic characteristics of the body by supplying energy to the near-surface flow region

The main objective of the present study is to demonstrate the possibility of actively influencing the position of the bow shock wave and the main parameters of supersonic flow over a blunt body in xenon by organizing a gas discharge near the front surface of the body in the region between the body and the bow shock wave. The study examines the impact of plasma parameters, specifically the degree of ionization and degree nonequilibrium, along with the discharge current and power, on the bow shock position in the steady flow mode. The research is carried out using both experimental and numerical methods. The findings may prove valuable in the development of new energetic methods for flow and flight control.

2. Experimental Setup and Results Obtained

 doi:10.20944/preprints202410.1285.v1

2.1. The Experiment Arrangement

The experimental part of the research was carried out on a test bench created on the basis of a shock tube with a gas-dynamic tract diameter of 5 cm. Figure 1 shows the scheme of the experimental setup. The high-pressure chamber (HPC) (1) 1 m long, designed for the pressure of pushing gas up to 100 atm, is separated from the low-pressure chamber (LPC) (2), 4.5 m long, by a diaphragm block (3) with an aluminum diaphragm, 0.4 mm thick. The chambers are preliminarily pumped out by separate pumps to a pressure of 10^{-3} Torr, then the working gas xenon is pumped into the LPC to an initial pressure of 30 Torr, and the pushing gas is hydrogen in the HPC. The diaphragm ruptures when the pressure in the HPC reaches 27 atm, which leads to the formation of a shock wave with a Mach number M_1=8, which, propagating along the LPC, compresses the working gas and creates a plug of shock-compressed gas. The LPC is connected to the working chamber (4), which contains a flat reflective supersonic nozzle with a wall angle of 11^0 relative to the axis and a width of 36 mm. The working chamber is separated from the LPC by a thin lavsan diaphragm (5). The shock-compressed working gas is decelerated at the end of the LPC, is ionized and after the separating diaphragm breaks, through an inlet slit 5 mm high with braking parameters enters the nozzle, where the supersonic flow is accelerated. The working chamber is connected to the damper tank (6), where the exhaust gas is discharged.

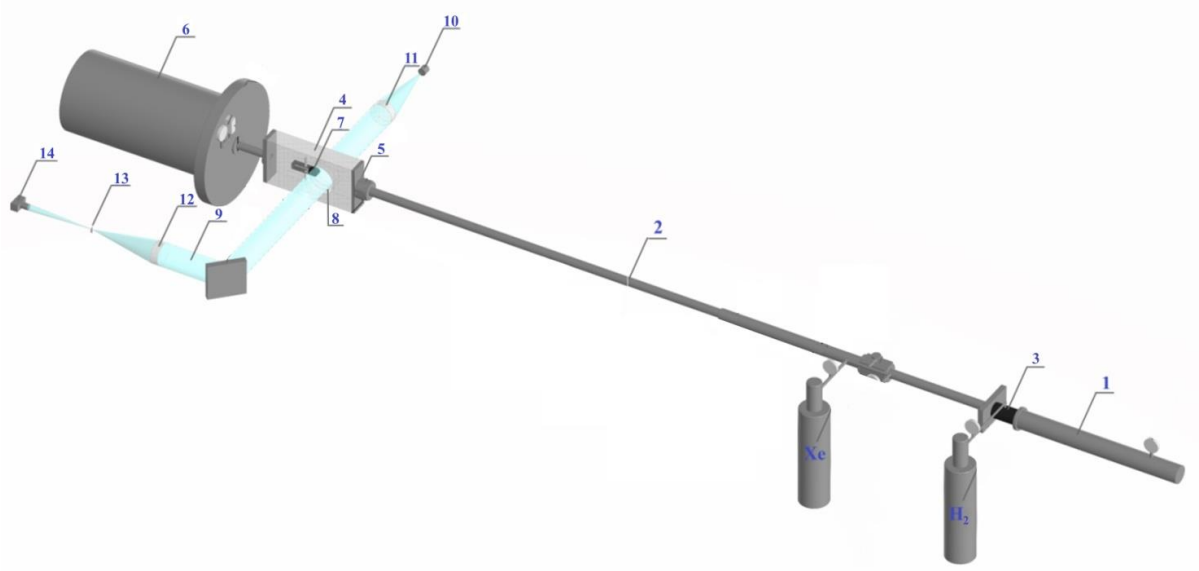

Figure 1. Scheme of the experimental bench.

At a distance of 20 cm from the nozzle entrance, where the flow reaches the Mach number M_∞=6.8, a blunt semi-cylindrical model (7) with a blunting radius of 15 mm is located on its axis. The model is clamped between two viewing side glasses (8), the width of the model corresponds to the channel width of 36 mm. A photograph of the model in the nozzle is shown in Figure 2a. Copper electrodes 5 mm wide and 30 mm long are mounted in the model at the top and bottom in the transition area of the cylindrical part to the horizontal, as shown in Figure 2b. The electrodes are connected to an external voltage source that forms a gas-discharge current near the front blunt edge of the model. The value of the voltage supplied to the circuit can be changed, thereby changing the intensity of the gas discharge. The gas discharge current is closed at the moment when ionized working gas enters the area between the electrodes.

 doi:10.20944/preprints202410.1285.v1

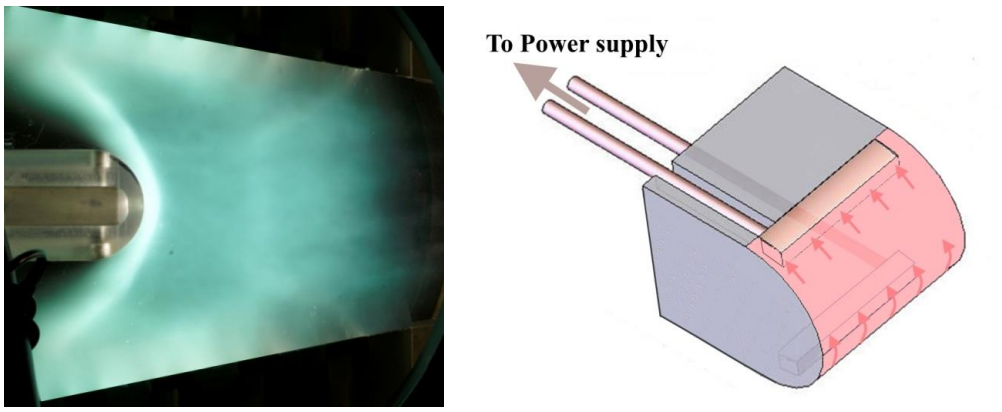

a) b)

Figure 2. The location of the model in the nozzle (a) and the shape of the studied model (b).

The flow patterns around the model are visualized by the schlieren system (9), where a pulsed semiconductor laser with a wavelength of 656 nm and pulse duration of 30 ns is used as a light source (10), which is the exposure time of the pattern. The source is located at a focal distance from the input lens (11), which creates a parallel beam of light shining through the working area with a diameter of 100 mm in the area of the model location. Then the light is focused by the output lens (12), creating an image of the input slit in the area of the knife location (13), as well as an image of the model on the recording matrix of the digital camera (14). The knife blocks half of the transmitted light, which creates a background of illumination at the model image on the camera matrix. During the flow around body, the light from the source is refracted on density gradients, blocked by the knife or passes over it, visualizing gas-dynamic discontinuities, including the bow shock wave arising during supersonic flow around the model under study. A photograph of the experimental setup is shown in Figure 3.

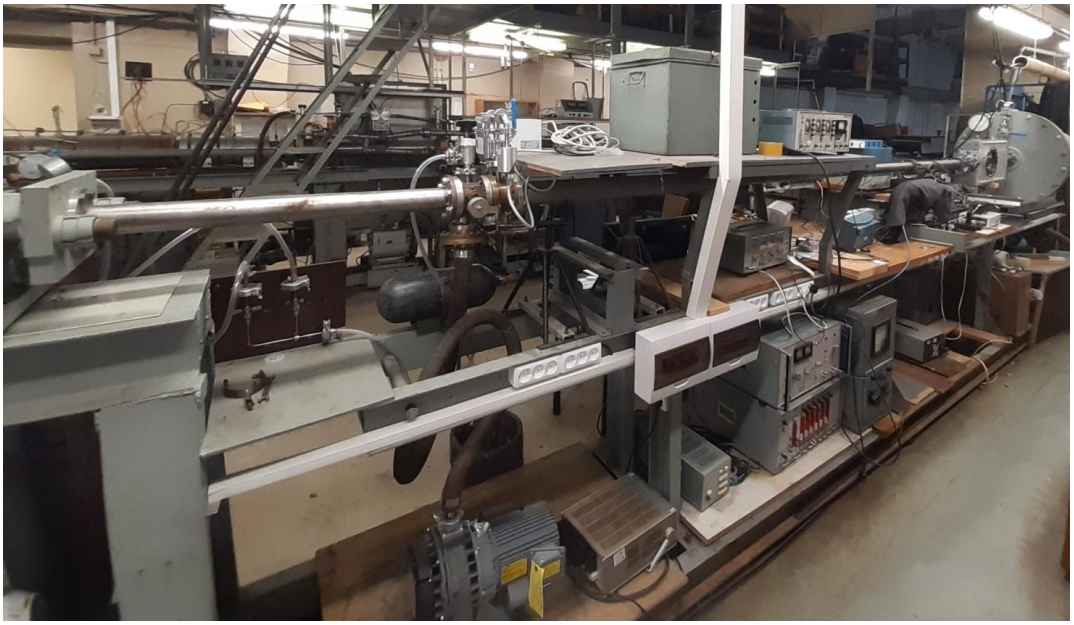

Figure 3. Photograph of the experimental bench.

2.2. Characteristics of the Surface Discharge

 doi:10.20944/preprints202410.1285.v1

To create a gas discharge near the leading edge of the body during its flow around, voltage from a specially made LC circuit is supplied to the electrode circuit before the experiment. As soon as the ionized gas, as a conducting medium, enters the area of the applied electric field, the gas discharge current is closed in the interelectrode gap. The LC circuit is designed to form a rectangular current pulse with duration of 600 μs, corresponding to the duration of the ionized flow. The impact begins at the moment the flow begins and the formation of the bow shock wave occurs already in the presence of the gas discharge zone. When braking at the body surface, the kinetic energy of the flow is converted into thermal energy, behind the bow shock wave the gas is ionized, its density and temperature increase, and the temperature state becomes close to equilibrium. The gas discharge increases both the degree of ionization in the area between the shock wave and the model, and the temperature of the electrons and gas as a whole, changing the degree of nonequilibrium. These processes will affect the adiabatic index of the medium, and consequently the gas-dynamic parameters of the flow.

Figure 4a shows the volt-ampere characteristic of the surface gas discharge. The voltage U_{pl} on the interelectrode gap changes in the range of 80-140 V, which creates a gas-discharge current I from 300 to 1200 A. The characteristic is almost linear, the extrapolation line intersects the voltage axis in the region of 60 V, which indicates the magnitude of the voltage drop when the current is closed, which occurs when electrons are emitted from the cathode surface. The power P input into the discharge depending on the resulting gas-discharge current is shown in the graph of Figure 4b. It is evident that the power supplied to the impact zone changes from 30 to 160 kW.

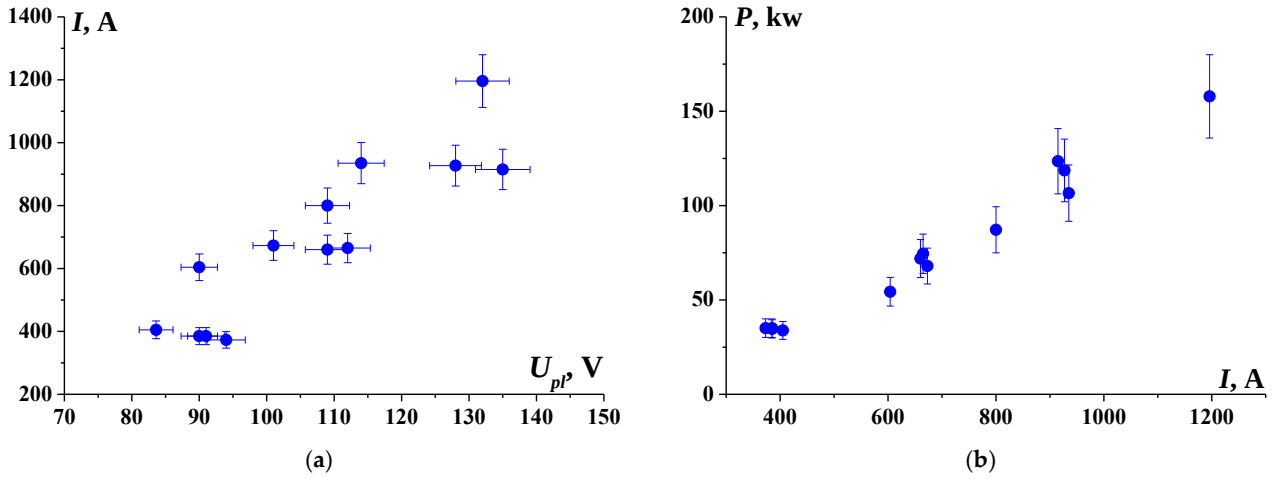

Figure 4. Volt-ampere characteristic of a gas discharge at the surface of a model (a); power input into the discharge (b).

The average plasma conductivity $\langle\sigma\rangle$ determined by the volt-ampere characteristics in the impact zone is shown in Figure 5a, the conductivity increases proportionally to the gas-discharge current. The resulting average electron concentration $\langle n_e \rangle$, estimated by the value of the discharge current and the values of electron mobility in the xenon gas-discharge medium [27], is shown in Figure 5b. The electron concentration increases in the range of $1.5 \div 6 \cdot 10^{22}$ m^{-3} as the discharge intensity increases in the impact zone.

 doi:10.20944/preprints202410.1285.v1

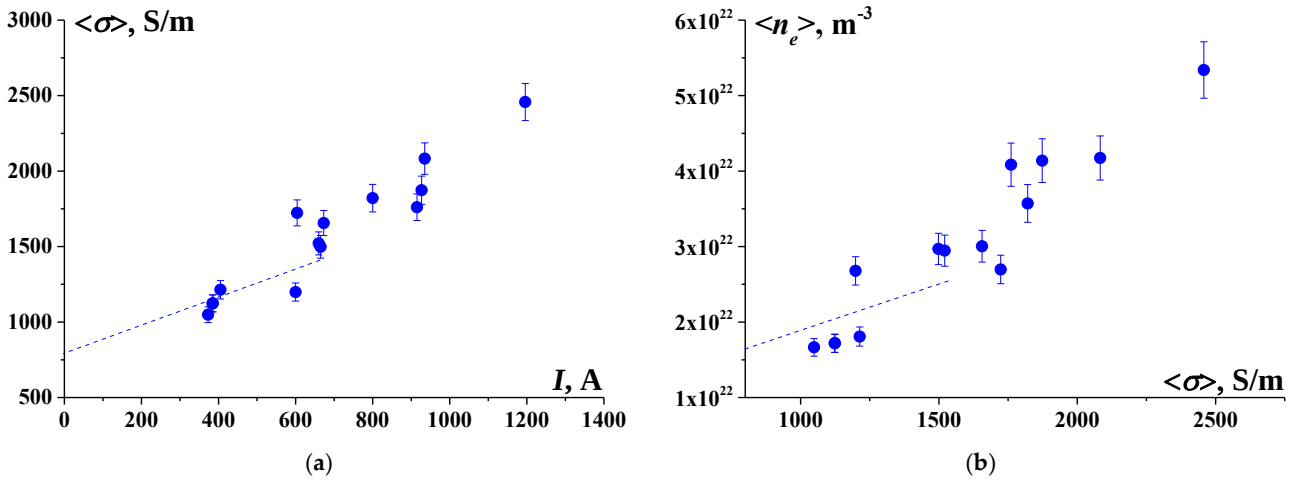

Figure 5. Dependence of the average plasma conductivity in the discharge core on the gas-discharge current (a) and the average values of electron concentration obtained in the discharge (b).

Figure 6 shows a typical oscillogram of the current in the discharge area (red curve), and the same graph shows the plasma conductivity in the interelectrode gap corresponding to this current (blue curve). It is seen that the duration of the impact corresponds to the flow duration of about 500-600 μs, and the parameters in the impact zone change slightly during the steady-state flow. The red dotted line shows the average value of the gas-discharge current; the black dotted lines limit the possible error in measuring the current to about 10%. The lower curve on the graph shows the time of switching on the laser pulse, i.e. the moment of fixing the schlieren flow pattern at the model, the flow pictures are taken at the stage of steady-state flow 350 μs after its start.

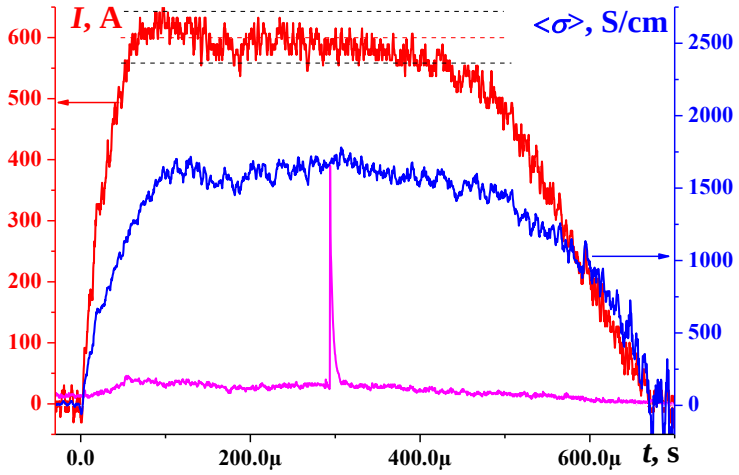

Figure 6. Oscillograms of gas discharge current and plasma conductivity in the area of the plasma impact (here *t* is the time counted from the moment of the flow reaching the front surface of the body).

Schlieren flow patterns of the model, showing the position of the bow shock wave at different discharge powers supplied to the area between the shock wave and the model, are shown in Figure 7. For clarity, the schlieren flow pattern in the absence of impact is shown at the bottom of the photographs. It is evident that with an increase in the discharge intensity, the position of the bow shock wave changes, it moves away from the body, the distance between it and the leading edge of the model increases, while both the shock wave configuration and the flow parameters, such as aerodynamic drag and dynamic load, change. As the presented studies have shown, the position of the bow shock wave at such action is determined not only by thermal effects, but also by plasma

 doi:10.20944/preprints202410.1285.v1

parameters in the impact zone, namely, the degree of ionization and the degree of nonequilibrium, which directly affect the adiabatic index of the medium.

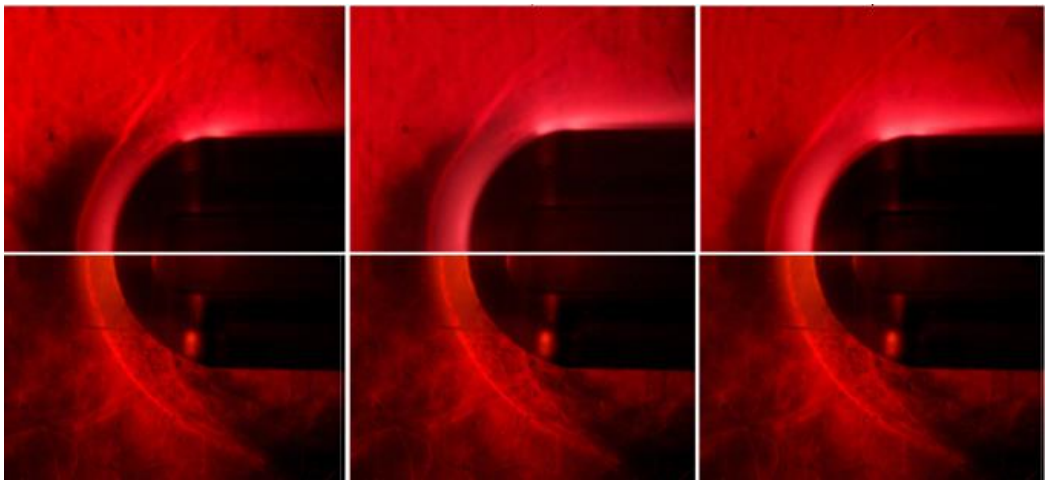

a) b) c)

Figure 7. Change in the flow pattern with increasing discharge intensity for a surface discharge in xenon; a) *I*=370 A, *P*=35 kW; b) *I*=670 A, *P*=68 kW; c) *I*=915 A, *P*=124 kW.

The discharge zone localization area for further calculations was determined by the plasma's own glow in the discharge. Figure 8 shows photographs of the discharge near the body taken through a red filter. In the numerical simulation, the discharge area was limited by a semi-cylinder with the radius of *R*=18 mm, while the discharge zone width was *x*=3 mm.

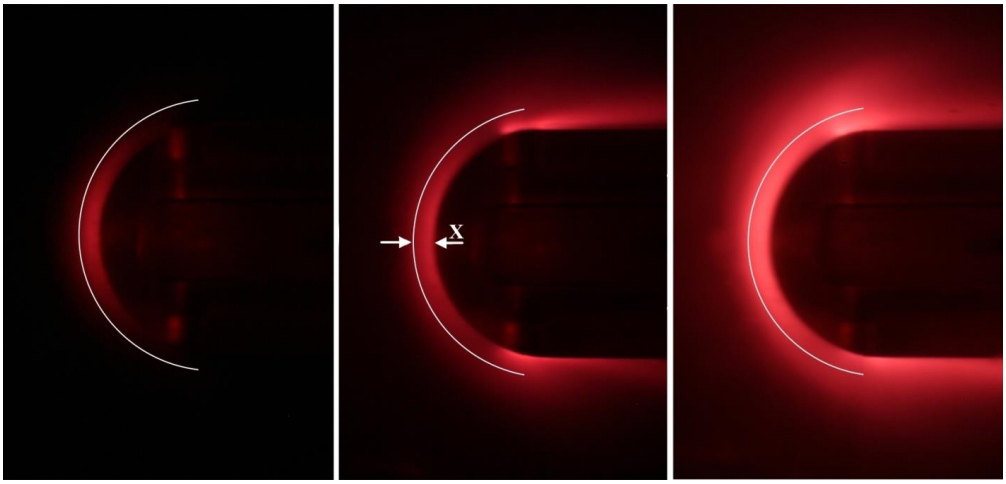

a) b) c)

Figure 8. Plasma's own glow during surface discharge; a) *I*=0; b) *I*=370 A, *P*=35 kW; ; c) *I*=915 A, *P*=124 kW.

2.3. Calculation of Plasma Parameters in the Accelerating Nozzle

Xenon was chosen as the working gas, as it is heavier, easily ionized and slowly relaxing gas. When calculating the parameters in the supersonic nozzle, the initial conditions were taken to be the values in the critical section equal to the braking parameters. When determining the initial conditions, it was assumed that there was ionization and thermodynamic equilibrium in the critical section, determined by the electron temperature T_{ecr}, which was assumed to be 10% higher than the temperature of the heavy component T_{hcr}. The supersonic flow in the nozzle was calculated in the

 doi:10.20944/preprints202410.1285.v1

approximation of a two-temperature plasma with nonequilibrium ionization during three-particle recombination.

The results of calculations of pressure p, gas temperature T_h and electrons T_e, conductivity σ and degree of ionization α are shown in Figure 9. All values are given in relation to the corresponding values of these quantities in the critical section: X_{cr}=1.42·10^{-2}m, M_{cr}=1.01, T_{hcr}=7700K, T_{ecr}=8700K, σ_{cr}=2500S/m, α_{cr}=1.5·10^{-2}, n_{hcr}=0.9·10^{25}m^{-3}. During expansion in the nozzle, a temperatures separation occurs due to the relatively slow relaxation of xenon, the electron temperature drops much more slowly than the gas temperature, the gas remains ionized with a nonequilibrium temperature distribution. As a result, a supersonic flow of nonequilibrium ionized xenon plasma with the following parameters flows onto the model: X=0.23m, T_h=1200K, T_e=3926K, σ=700S/m, α=0.0018, p=3.1·10^{3}Pa, n_h=1.87·10^{23} m^{-3}, n_e=3.37·10^{20}m^{-3}. The glow of xenon plasma is clearly visible in Figure 2a.

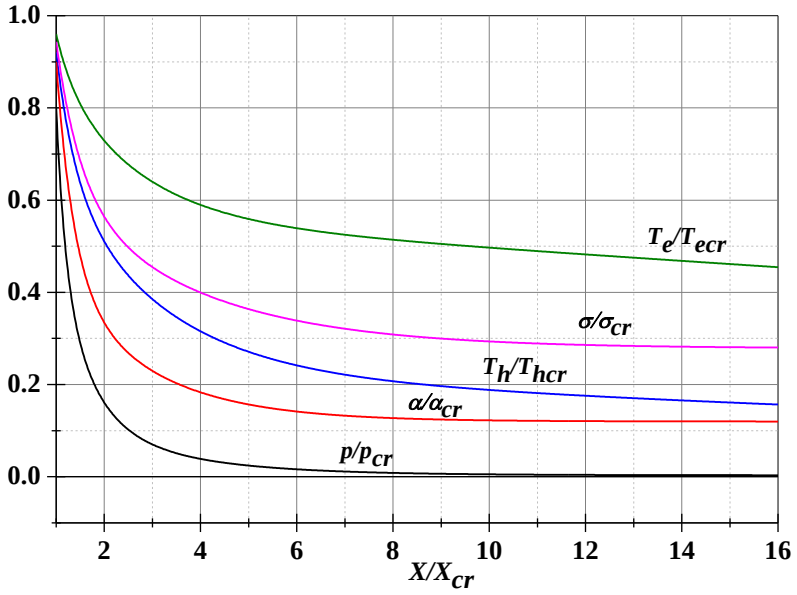

Figure 9. Distribution of the main flow parameters along the nozzle axis.

In addition, according to the theory of K. Burm et al. [24], one of the main parameters that determines the nature of supersonic flow is the adiabatic index γ in ionized nonequilibrium plasma differs significantly from the ideal theory (γ =c_p/c_v) and depends on bough the degree of nonequilibrium θ =T_h/T_e, and the degree of ionization α =n_e/n_h [24].

Figure 10 shows the dependence of the adiabatic index on the degree of nonequilibrium according to the theory [24] for the values of gas temperature and the degree of ionization corresponding to the calculated values in the flow at the nozzle exit in the region of the model location. The dashed lines show the value of the degree of nonequilibrium and the corresponding value γ=1.217, which was taken as the value of the adiabatic index in the supersonic flow incoming on the body.

 doi:10.20944/preprints202410.1285.v1

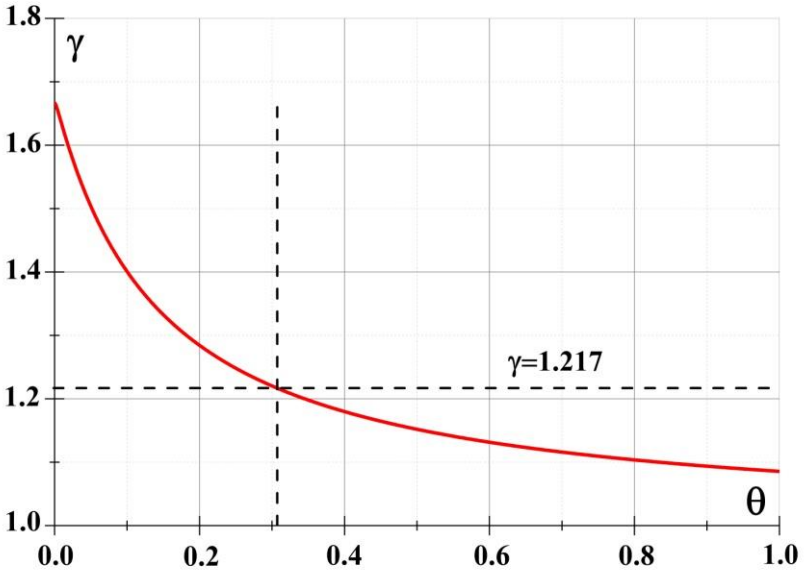

Figure 10. Dependence of the adiabatic index on the degree of nonequilibrium at T_h=1200K and α=0.0018.

During braking near the leading edge of the model, the flow is additionally ionized, its parameters approach thermodynamic equilibrium. As a result, the degree of nonequilibrium θ becomes of the order of unity, and the degree of ionization α increases to $1.9 \cdot 10^{-2}$, which leads to an increase in the adiabatic index in the region between the bow wave and the front surface of the body. The initial value of γ in the impact zone in the absence of a gas discharge was evaluated by the same approach as γ_s =1.258.

3. Numerical Simulations of the Impact of a Surface-Energy Deposition on the Bow Shock Wave and Aerodynamic Characteristics of a Model

3.1. Methodology and Statement of the Problem

In the experiment, the ionized flow moves out of the shock tube, reaches the body, and causes the ignition of a discharge between the electrodes located on the body, to which voltage is applied. When the flow reaches the body, the formation of the bow shock wave begins, which passes through the gas-discharge plasma impact zone. In this case, additional ionization occurs in front of the body due to an increase in temperature behind the shock wave front. It should be noted that this additional ionization is present in the steady flow in the absence of discharge action, as well. In the calculations, it is assumed that the hot impact zone of ionized gas in front of the body occurs instantly, which is due to the difference in the time scales of discharge and gas-dynamic phenomena. Thus, in the simulation, the discharge action is described by the action of a volumetric gas region with the increased energy and changed adiabatic index. The scheme of the numerical approach to the study of an impact of a near-surface energy deposition on a supersonic flow past a plate blunted by a cylinder is shown in Figure 11. Here the discharge action impact zone is marked by red.

Preprints.org (www.preprints.org) | NOT PEER-REVIEWED | Posted: 16 October 2024 doi:10.20944/preprints202410.1285.v1

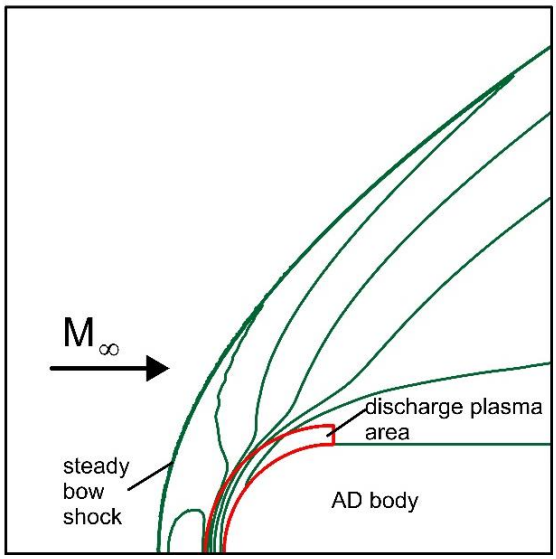

Figure 11. Statement of the problem (schematic).

The simulations are based on the Navier-Stokes equations for perfect viscous heat conductive gas (xenon); the ratio of specific heats (adiabatic index) was a fitting parameter for different values of the specific discharge power q (power on the unit of mass). The flow is supposed to be parallel to the axis of symmetry. The full Navier-Stokes system of equations in the divergent form for the dimensionless variables [28] is solved numerically:

$$\frac{\partial \mathbf{U}}{\partial t} + \frac{\partial (\mathbf{F}+\mathbf{F}_v)}{\partial x} + \frac{\partial (\mathbf{G}+\mathbf{G}_v)}{\partial y} = \mathbf{H} \qquad (1)$$

$$\mathbf{U} = \begin{pmatrix} \rho \\ \rho u \\ \rho v \\ E \end{pmatrix}, \mathbf{F} = \begin{pmatrix} \rho u \\ p + \rho u^2 \\ \rho uv \\ u(E+p) \end{pmatrix}, \mathbf{G} = \begin{pmatrix} \rho v \\ \rho uv \\ p + \rho v^2 \\ v(E+p) \end{pmatrix}, \mathbf{H} = \begin{pmatrix} 0 \\ 0 \\ 0 \\ \rho q \end{pmatrix},$$

$$\mathbf{F}_v = -\begin{pmatrix} 0 \\ \mu/\mathrm{Re}(4/3u_x - 2/3v_y) \\ \mu/\mathrm{Re}(v_x + u_y) \\ \mu\pi_1/\mathrm{Re} + (1/\mathrm{N})kT_x \end{pmatrix}, \mathbf{G}_v = -\begin{pmatrix} 0 \\ \mu/\mathrm{Re}(v_x + u_y) \\ \mu/\mathrm{Re}(4/3v_y - 2/3u_x) \\ \mu\pi_2/\mathrm{Re} + (1/\mathrm{N})kT_y \end{pmatrix}$$

$$\pi_1 = u(4/3u_x - 2/3v_y) + v(v_x + u_y), \pi_2 = v(4/3v_y - 2/3u_x) + u(v_x + u_y)$$

$$E = \rho(\varepsilon + 0.5(u^2 + v^2)), \mathrm{N} = \mathrm{RePr}(\gamma - 1)/\gamma.$$

Here q is the specific power in the area of higher gas energy formed by the discharge, ε is the specific internal energy,

$$\varepsilon = p/(\rho(\gamma - 1)).$$

The freestream Mach number $M_\infty = 6.8$ and the Reynolds number Re=4559, the Prandtl number Pr=0.623.

The dependence of dynamic viscosity μ on temperature is supposed as:

$$\mu = T^{0.5}.$$

The coefficient of heat conductivity k is supposed to depend on temperature by the same way:

$$k = T^{0.5}.$$

 doi:10.20944/preprints202410.1285.v1

The problem is solved in dimensionless variables, which are expressed through dimensional variables (designated by the index "dim") as follows:

$$t = \frac{t_{dim}}{t_{n,}}, x = \frac{x_{dim}}{l_{n,}}, y = \frac{y_{dim}}{l_{n,}}, u = \frac{u_{dim}}{u_{n,}}, v = \frac{v_{dim}}{u_{n,}},$$

$$\rho = \frac{\rho_{dim}}{\rho_n}, p = \frac{p_{dim}}{p_n}, T = \frac{T_{dim}}{T_n}.$$

The following scaling coefficients were used in the calculations:

$$\rho_n = \rho_\infty, p_n = p_\infty, l_n = D, T_n = T_\infty, u_n = (p_\infty/\rho_\infty)^{0.5}, t_n = l_n/u_n,$$

where the index ∞ defines the free stream parameters. Further figures, where not specified, are given in dimensionless variables.

Initial conditions are the flow with freestream values of density ρ_∞, pressure p_∞, and velocity u_∞. We suppose that the adiabatic index in the oncoming flow γ=1.217, and the adiabatic index in the plasma area created by the discharge in front of the body is γ_s=1.258. Therefore, the problem is solved taking into account the initial gas ionization.

The boundary conditions have a sense of the absence of according normal flows on the boundaries of the body:

$$\frac{\partial p}{\partial n} = 0; \ \frac{\partial T}{\partial n} = 0; \ \boldsymbol{U} = 0.$$

The conditions of the absence of reflection in the normal directions are set at the exit boundaries of the computation domain:

$$\frac{\partial p}{\partial n} = 0; \ \frac{\partial T}{\partial n} = 0; \ \frac{\partial \boldsymbol{U}}{\partial n} = 0.$$

The near-surface energy deposition is modelled via the creating a stationary region of higher gas energy using the right part in the equation of energy in (1), where q is the specific power in this region (this area is noted by red in Figure 11). The width of this area in the x-direction is supposed to equal to $0.1D$, which is in accordance with the experimental Schlieren images (see Figure 8). We supposed that this area arises instantly and it is determined via the initial conditions and the value of q.

The simulations are performed using a computational code that employs complex conservative difference schemes [29]. The schemes have the second order of approximation, both in space and in time. The five-point stencil from Lax's scheme is used for scheme construction, resulting in staggered and uniform grids throughout the computational domain. To increase the order of approximation in the development of the schemes, the differential consequences of system (1) are utilized for partial spatial derivatives on x and y. The boundaries of an AD body are introduced into the calculation area without breaking the conservation laws in it. The construction details of these schemes within the computational domain, and in the vicinity of the AD body boundaries are presented in [29].

In an enlarged format, Figure 2 illustrates the position of the body's front part on the difference grid. The staggered numerical grids employed in the calculations feature a node spacing of $2h_x$ and $2h_y$ at each time level (where h_x and h_y denote the spatial steps in the x- and y-directions, respectively). The selection of the time step is performed using the Courant-Friedrichs-Levy criterion. It should be noted that a number of test cases pertaining to the numerical methods employed, a comparison with the experimental results, and the developed software are presented in [29].

 doi:10.20944/preprints202410.1285.v1

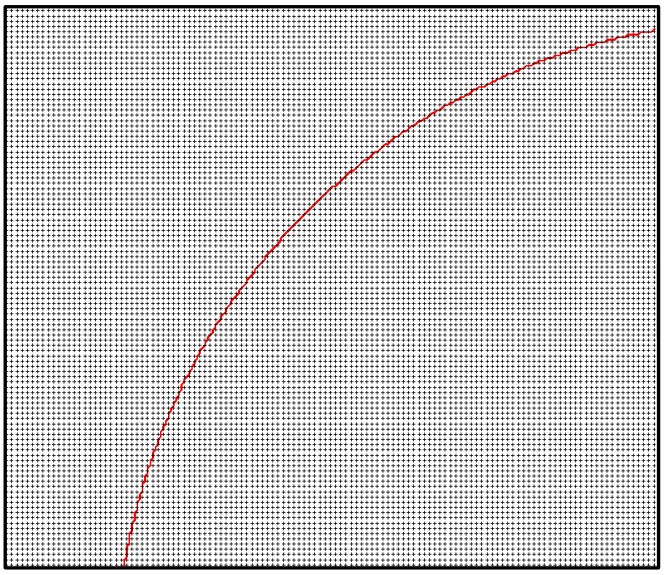

Figure 12. The position of a part of the front surface of the body on a computational grid (enlarged, every forth node is shown).

3.2. Analysis of the Grid Convergence

A study of the grid convergence of the difference method used was conducted. The results were obtained on three different grids. The characteristics of these grids are presented together with the relative errors in the stagnation parameters (at the center of the cylinder surface) related to the theoretically values obtained with the help of the Bernoulli's relation (Table 1). Here the dimensions of the grids are specified counting the middle node of the stencil.

Table 1. Grid convergence analysis*.

Difference grid	A number of working nodes in the grid	The values of time steps h_x, h_y	Relative error, p_t: $abs(p_t - p_{t\ theor})/ p_{t\ theor}$ ×100%	Relative error, ρ_t: $abs(\ _t - \ _{t\ theor})/\ _{t\ theor}$ ×100%
Grid 1	5.625×10^6	$h_x=h_y=0.001$	0.091%	1.080%
Grid 2	2.758×10^6	$h_x=h_y=0.0014286$	1.011%	5.798%
Grid 3	9.0×10^5	$h_x=h_y=0.0025$	1.609%	6.608%

*The calculations were conducted for M=6.98 and $\gamma=\gamma_s=5/3$.

Figure 13 shows a comparison of the density fields in isochores obtained on three grids Grid1, Grid2, Grid3. From the analysis of the presented fields, we can conclude that there is grid convergence in the position and shape of the bow shock wave, as well as in the flow structure inside the shock layer.

Preprints.org (www.preprints.org) | NOT PEER-REVIEWED | Posted: 16 October 2024 doi:10.20944/preprints202410.1285.v1

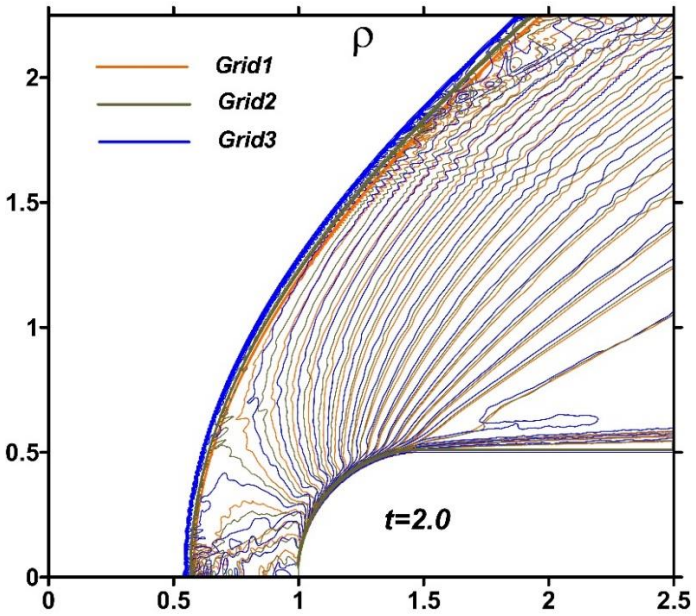

Figure 13. Density fields in isochores obtained on the three difference grids.

Figure 14 shows the dynamics of density and pressure at the critical point, ρ_t and p_t (at the center of the cylindrical surface of the body) (Figures 14a and 14b), as well as the x-coordinates of the bow shock wave X_{bsw} and the drag force of the frontal surface F (Figures 14c and 14d) in the process of establishing a steady-state flow regime. Relative errors for the stagnation parameters are presented in Table 2. These results also confirm the presence of grid convergence for the used configuration of the numerical experiment. In the calculations the Grid1 (h_x=h_y=0.001) is used.

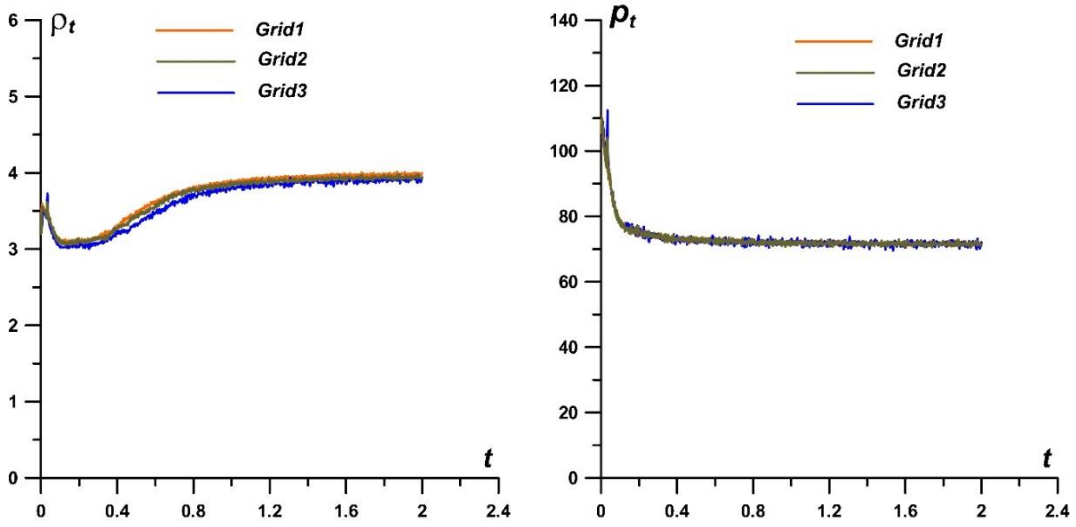

a) b)

 doi:10.20944/preprints202410.1285.v1

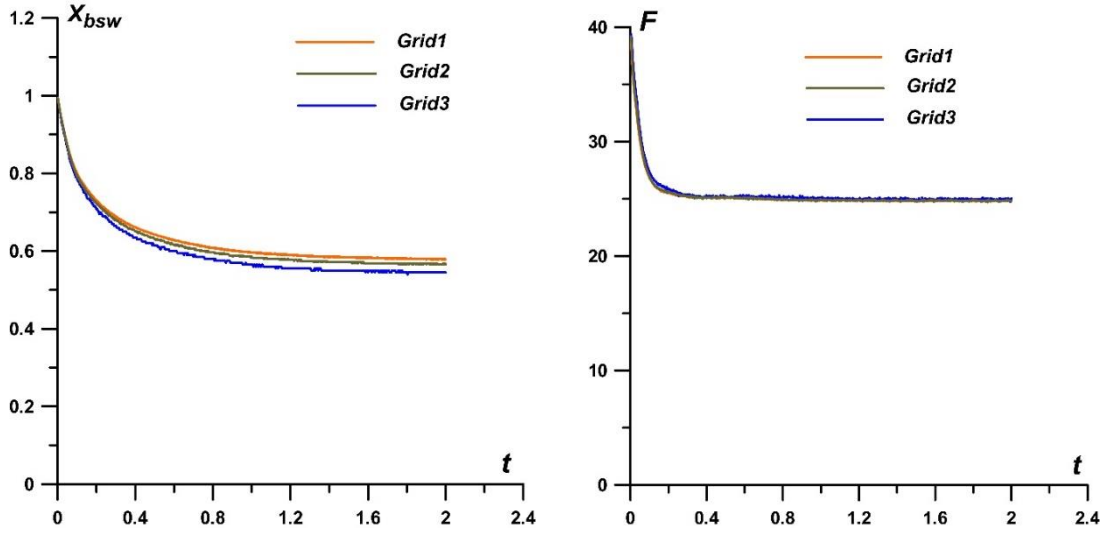

c) d)

Figure 14. Dynamics of flow parameters during establishment of a steady-state flow regime, obtained on three difference grids: a), b) density and pressure at the central point of the cylindrical surface of the body; c) *x*-coordinate of the bow shock wave; d) drag force of the frontal surface of the body.

3.3. Results of the Simulations

The defining flow parameters used in the experiments and simulations are presented in Table 2.

Table 2. Defining parameters of the oncoming flow and normalizing coefficients.

Description	Dimensional value	Dimensionless value	Normalizing coefficient
Freestream Mach number M_∞		6.8	
Adiabatic index in freestream flow γ		1.217	
Reynolds number Re		4558.9	
Prandtl number Pr		0.623	
Freestream gas pressure p_∞	$3.1 \cdot 10^3$ Pa	1.0	$p_n = p_\infty$
Freestream gas density ϱ_∞	0.040793 kg/m^3	1.0	$\varrho_n = \varrho_\infty$
Freestream gas temperature T_∞	1200 K	1.0	$T_n = T_\infty$
Adiabatic index in oncoming flow γ_∞		1.217	
Specific power in the plasma region q			$q_n = p_n / (t_n \varrho_n) =$ $=0.698299 \times 10^6$ kW/kg
Body's diameter D	3×10^{-2} m	1.0	$l_n = D = 3 \times 10^{-2}$ m
Velocity u	2067.96 m/s	7.502	$u_n = (p_n / \varrho_n)^{0.5} =$ 275.668 m/s
Time t		1.0	$t_n = l_n / u_n = 108.827$ μs

In Figure 15, a comparison of the experimental image and numerical flow picture in isochors for the quasi-steady flow mode in the absence of the discharge impact is presented. The calculations are conducted with taking to account the initial ionization of the flow near the body behind the bow

 doi:10.20944/preprints202410.1285.v1

shock wave, γ=1.217, γ_s=1.258 (Figures 15–18). At the stagnation point the difference between the numerical and theoretical values (calculated using the Bernoulli relation) is 2.476% for density and 0.014% for pressure. We used the criterion for the evaluation of the relative errors in a form:

$$\mathrm{abs}(f_t - f_{t\,theor})/\, f_{t\,theor} * 100(\%),$$

where f_t and $f_{t\,theor}$ are the calculated value in the center point of a cylinder surface and the theoretical one.

Difference between the experiment and numerical values of the relation of the body radius to the stand-off distance (at the axis of symmetry), $0.5D/d$ is 15.8%. This difference, especially at the periphery, is related to the flow behavior in the expanding nozzle (and the approximately defined Mach number in the experiment). In this regard, in what follows we consider not the absolute, but the relative standoff of the bow shock wave from the body, focusing on the parameters on the axis of symmetry.

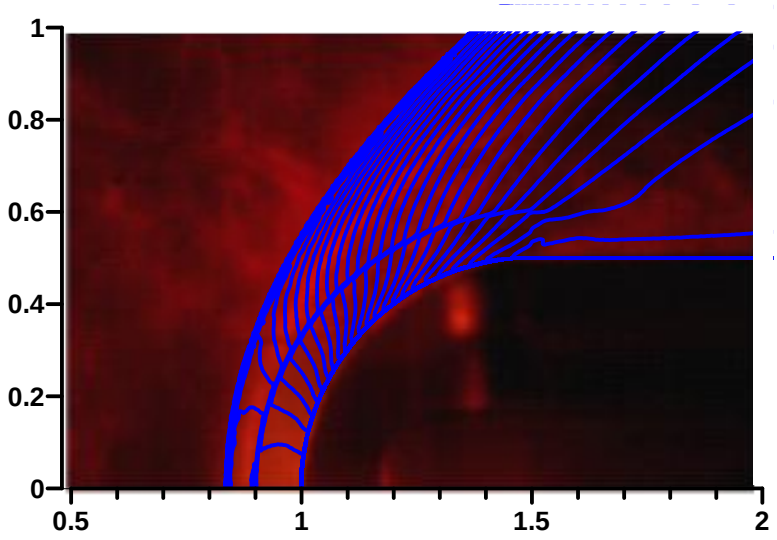

Figure 15. A comparison between the experimental and numerical flow pictures, γ=1.217, γ_s=1.258, q=0.

In Figure 16, the numerical fields of density, pressure, temperature, and local Mach number are presented for the steady flow mode (t=2.0) at q=0 (absence of the discharge). It can be seen that the initial ionization influences the flow temperature to a greater extent than to other parameters.

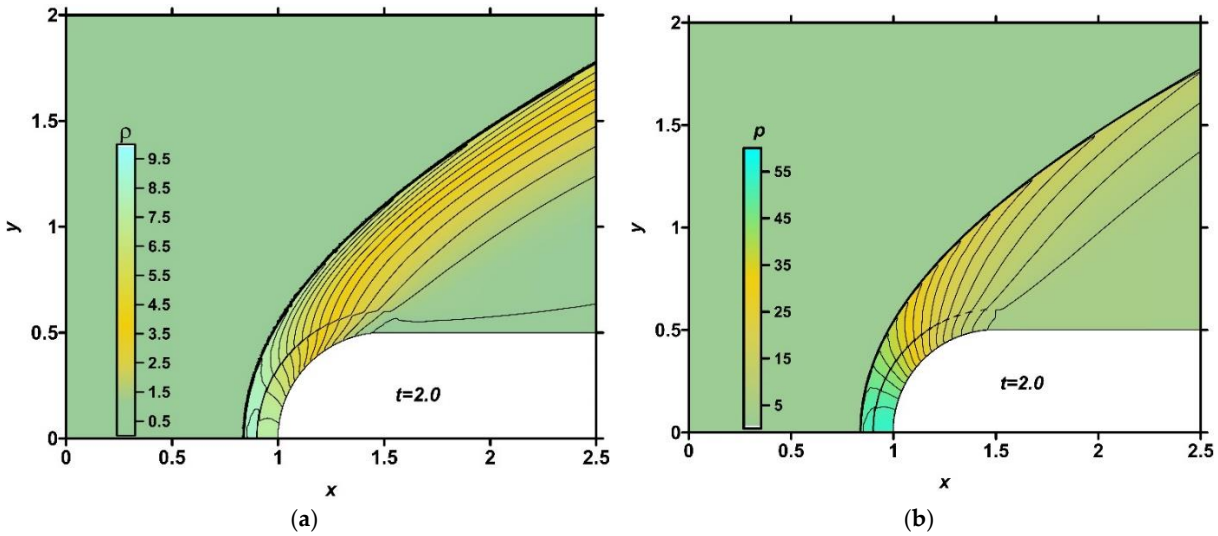

(**a**) (**b**)

 doi:10.20944/preprints202410.1285.v1

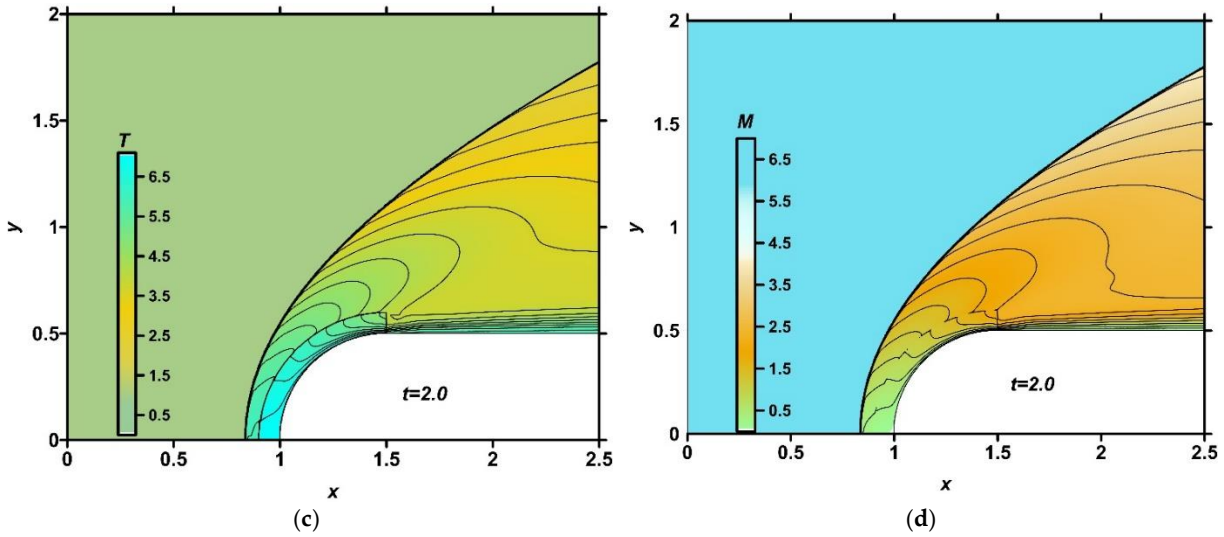

(c) (d)

Figure 16. Fields of density (a), pressure (b), temperature (c) and local Mach number (d) in the absence of a discharge, q=0, steady flow mode, t=2.0, γ=1.217, γ_s=1.258.

Figure 17 illustrates the results of simulations of the influence of the near-surface discharge energy impact zone the position of the bow shock at the steady state (t=2.0). Here we consider the case with the influence of the changed adiabatic index in the plasma region, γ=1.217, γ_s=1.258. In Figure 17a, the density fields for different values of the specific power are presented for the steady flow. It can be seen that the steady bow shock wave stand-off distance is greater for higher values of the specific power q. Figure 17b shows the dependence of the relative bow shock wave distance on the specific discharge power q. The mechanism of such a phenomenon is described in [26] for an air flow. This influence is connected with the fact, that the bow shock wave, during its formation, is moving throw already exsisting plasma heated area (due to the difference in time scales of the discharge plasma zone formations and gas dynamic processes). Thus, the parameters of the discharge zone influence the parameters of the forming bow shock wave at the unsteady stage, and as the result, at the steady stage, as well.

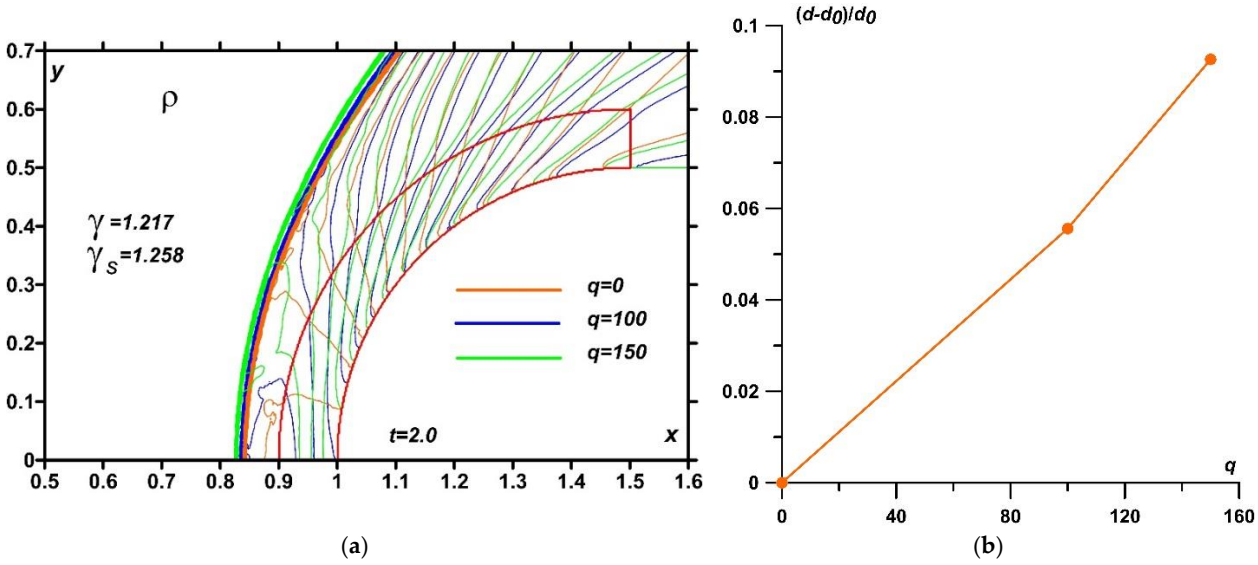

(a) (b)

Figure 17. a) Density fields in isochores for different values of specific power q; b) relative bow shock wave stand-off distance *vs* specific power; t=2.0, γ=1.217, γ_s=1.258.

Figure 18 illustrates the dynamics of density, pressure, temperature, and the relative drag force F/F_0 during the establishment of their stagnation values at the central point of the semi-cylinder for various values of q. It is seen from Figures 18(a)-18(c) that, at this point, pressure exhibits only slight

Preprints.org (www.preprints.org) | NOT PEER-REVIEWED | Posted: 16 October 2024 doi:10.20944/preprints202410.1285.v1

changes with an increase in specific power q, whereas the gas rarefaction significantly increases, resulting in a substantial rise in temperature. It should be highlighted that the relative drag force F/F_0 acting on the front surface decreases overall with the increase in the stand-off distance of the steady bow shock wave; this force is greater for higher values of q, as shown in Figure 18d.

Here the drag force is

$$F = \int_0^{0.5D} p_b dy,$$

where p_b is the pressure value at the cylindrical part of the body's surface, F_0 is the value of the drag force F without energy deposition.

Figure 18e illustrates the dynamics of the bow shock front position for varying values of q during the establishment of a steady flow. The position of the bow shock wave was determined by identifying the x-coordinate that corresponded to the maximum value of p_x at its front. Note that the fluctuations in the dependencies are due to the discreteness of the representation of the wave front in the difference cell, associated with the construction of the algorithm for tracking the front of the bow shock wave. Therefore, at the initial stage, when the bow shock is moving throw the region of the discharge plasma, the action of the energy source gradually increases the distance of the bow shock wave stand-off from the body, which is greater for higher values of the specific power. Subsequently, this increase affects the position of the bow shock wave in the steady state.

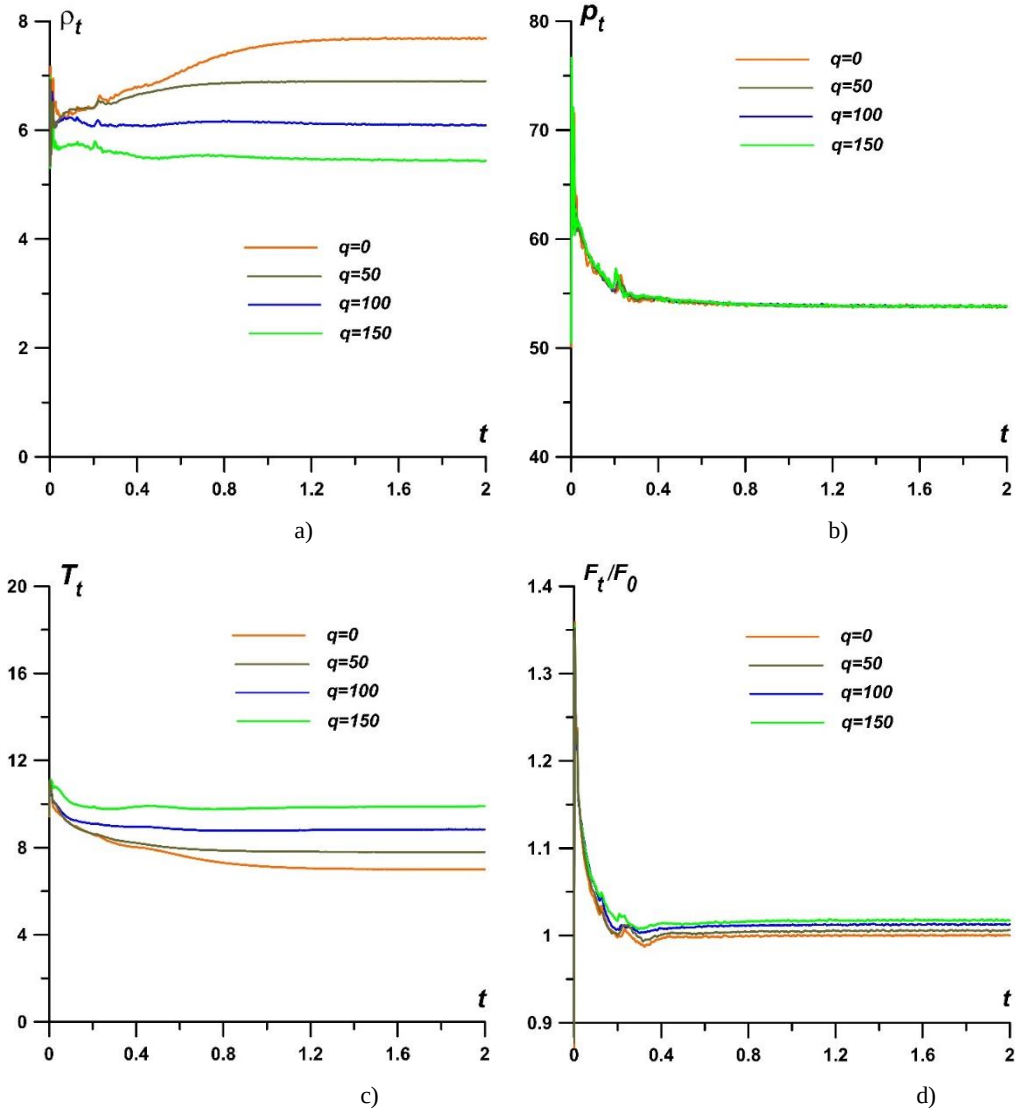

Preprints.org (www.preprints.org) | NOT PEER-REVIEWED | Posted: 16 October 2024 doi:10.20944/preprints202410.1285.v1

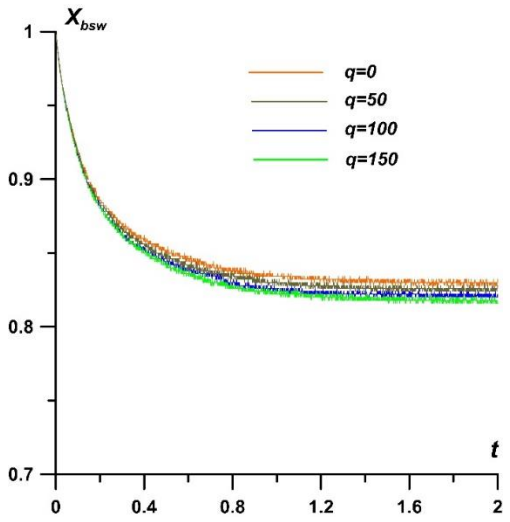

e)

Figure 18. Dynamics of density (a), pressure (b), temperature (c) at the stagnation point of the cylinder, relative drag force (d), end the x-coordinate of bow shock front for different values of q during the steady flow establishing (e); t=2.0, γ=1.217, γ_s=1.258.

In Figure 19, the fields of determining flow parameters (density, pressure, temperature, and local Mach number) are presented at q=200 and γ_s=1.29 for the steady flow mode. This case is corresponded to the strongest influence of the discharge plasma zone on the flow. A region of compressed gas with increased pressure and temperature forms behind the bow shock wave front, as well as in a case of lacking an energy source. However, due to the deposition of energy, an adjacent region of less dense gas is created in the vicinity of the front surface of the body, resulting in the formation of a layer with an elevated gas temperature. Moreover, it is notable that high-temperature subsonic zones develop in proximity to the horizontal boundaries of the body. These zones are also observable in the Schlieren images, as illustrated in Figure 7.

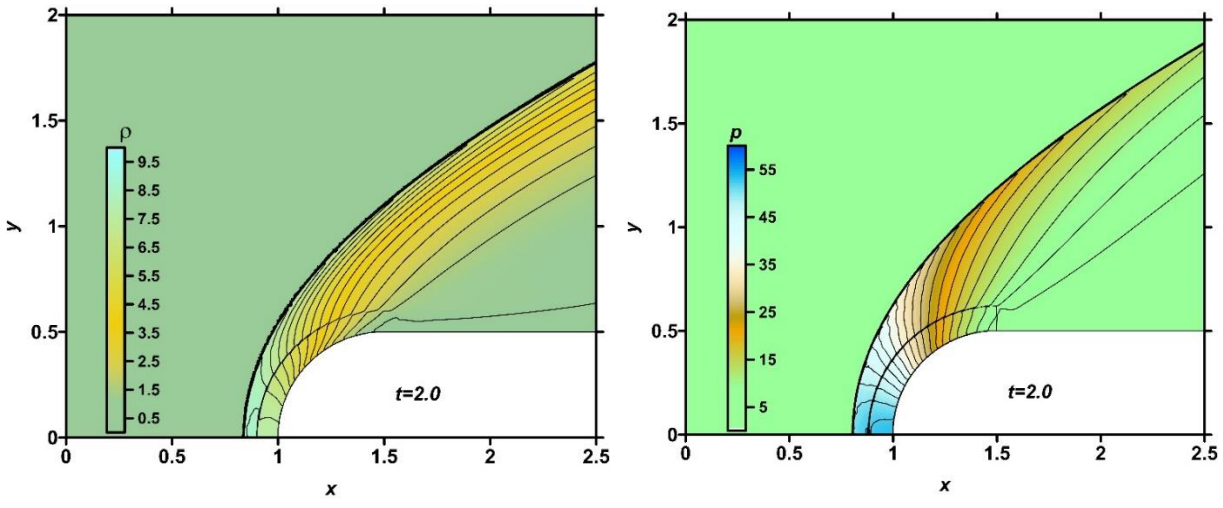

(**a**) (**b**)

 doi:10.20944/preprints202410.1285.v1

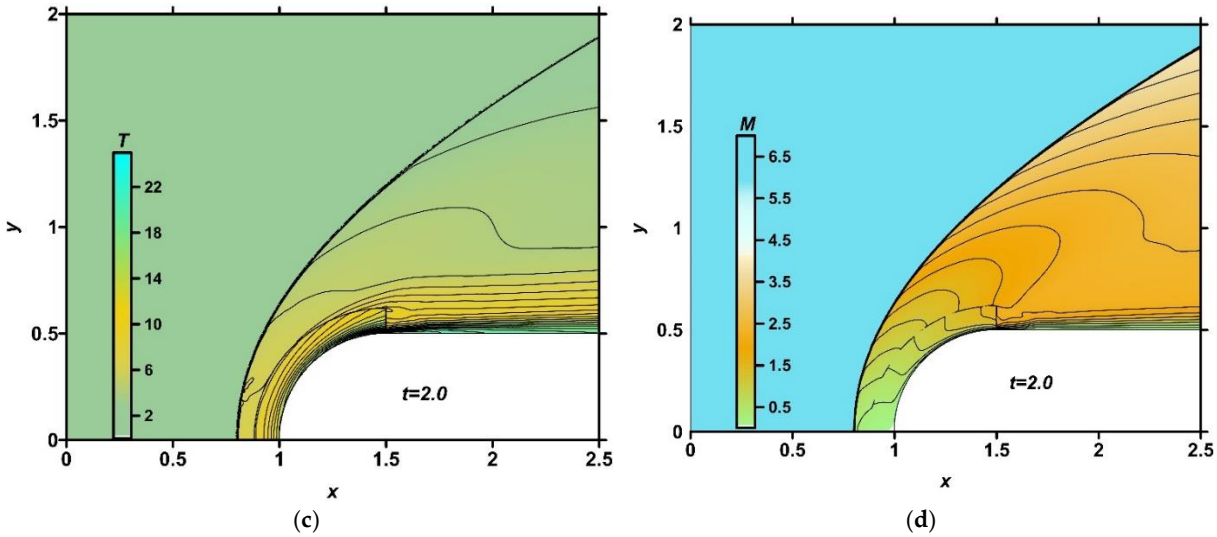

(c) (d)

Figure 19. Fields of density (a), pressure (b), temperature (c) and local Mach number (d) for q=200, γ_∞ =1.217, γ_s=1.29 steady flow mode, t=2.0.

Calculations indicated that significant changes in temperature and density occur in the near-surface region due to the discharge energy release. It was also showed that the adiabatic index γ_s influences the position of the bow shock wave in the steady flow regime. Density fields for steady flow modes at q = 100 and varying of γ_s values are presented in Figure 20a, illustrating that a higher γ_s corresponds to a larger stationary distance of the bow shock wave. Figure 20b shows the dependence of the relative steady bow shock stand-off distance on γ_s for q=100, indicating that changes in γ_s have a significant impact on the relative stand-off value of the steady bow shock wave.

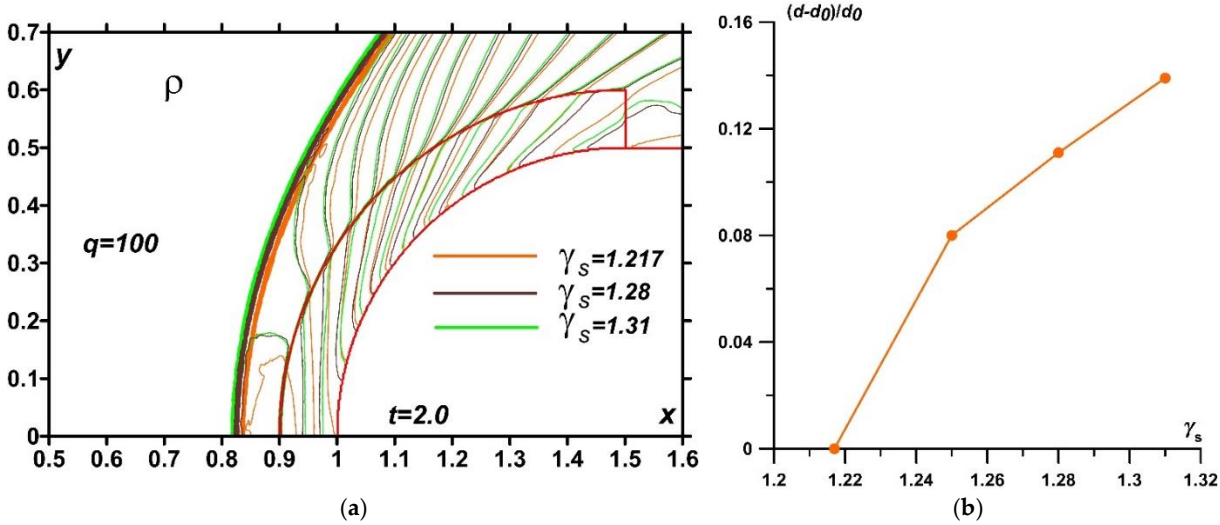

(a) (b)

Figure 20. Density fields in isochores for different values of adiabatic index in the xenon plasma area γ_s (a) (overlay of enlarged images) and relative bow shock wave stand-off *vs* γ_s (b); steady flow mode, t=2.0, q=100, γ=1.217.

4. Quantitative Comparison of the Experimental and Numerical Results

The calculated and experimental dependences of the relative value of the steady bow shock wave stand-off distance on the discharge power for the cases of taking into account the initial increased ionisation before the body and without this are presented in Figure 21. Here, in the simulation we used of the calculated value of average density in the discharge plasma zone. From Figure 21 one can see that approximately at $0<P<1.25\times10^5$W (which is corresponded to $0<I<915$A) the calculated and experimental values of the relative stand-off distance are in good agreement. So, it is

Preprints.org (www.preprints.org) | NOT PEER-REVIEWED | Posted: 16 October 2024 doi:10.20944/preprints202410.1285.v1

evident that the relative values of the stand-off distance at the steady flow mode is determined by two parameters, q and γ_s, and the adiabatic index generally increases with increasing current and discharge power. It can be seen that at the beginning stage, $0<P<5.42\times10^5$W (which is corresponded to $0<I<604$A) the dependence of the relative distance on the discharge power is close to linear. In addition, the oscillation of the relative stand-off distance was obtained at 1.25×10^5W$<P<8.66\times10^5$W (604A$<I<800$A). This oscillation can be explained by the fact that the adiabatic index γ_s is strongly dependent on the degree of ionization in this range of the discharge current, which can lead to both its increase and decrease (see, also, Part 5).

Besides, in Figure 21 the comparison is presented for the results obtained with taking into account the initial ionization ahead of the model (ruby red curve) and without it (orange curve). It can be concluded that when we take into account the initial ionization behind the model, the obtained the values of q differ for small discharge currents (and powers) at first slightly, and this difference increases (and becomes significant) with increasing discharge current. The values of the adiabatic index γ_s for small discharge currents differ by 3.4%-3.8%, and for larger currents the action of the initial ionization weakens, and these values differ by 1%-2%. In general, it can be concluded that taking into account primary ionization is important both for small currents (since for these values there is a noticeable difference in the values of γ_s) and for large currents, for which a large difference in the estimates of the specific power was obtained.

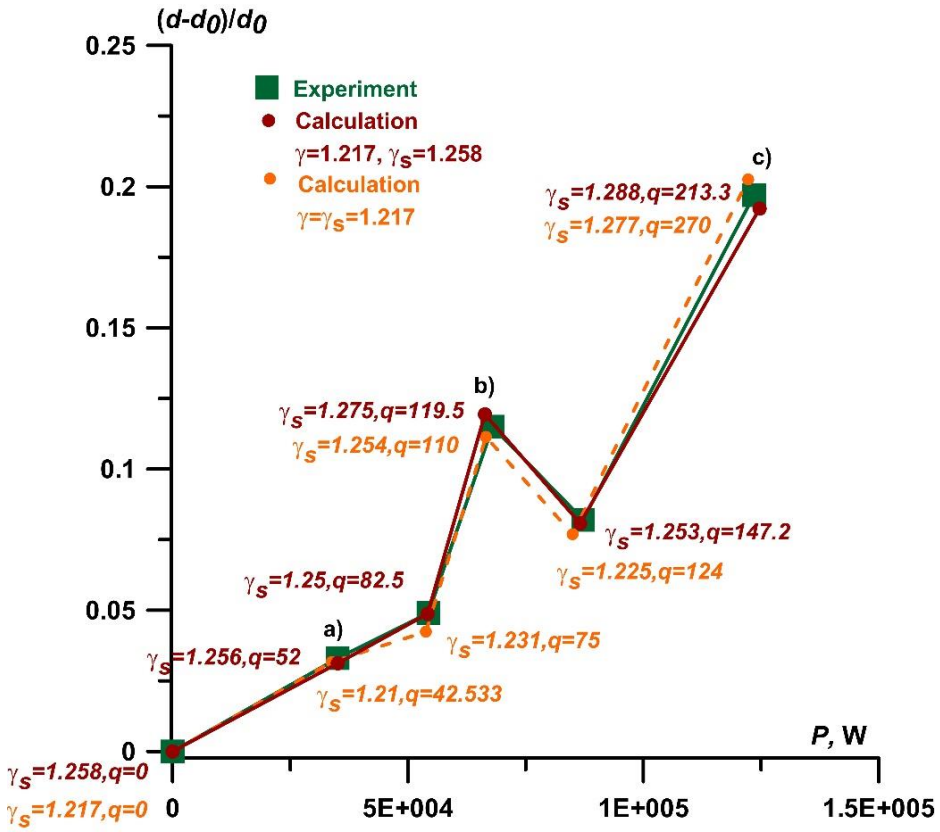

Figure 21. Dependence of the relative value of the steady bow shock stand-off distance on the discharge power.

Figure 22 demonstrates the according comparison of the numerical flow patterns and schlieren images of the near-surface discharge action in xenon. It is seen the good agreement of the numerical and experimental values in the locations of the bow shock waves on the axis of symmetry for the obtained parameters γ_s and q, evaluated sizes of the plasma area, and the established initial freestream flow conditions.

 doi:10.20944/preprints202410.1285.v1

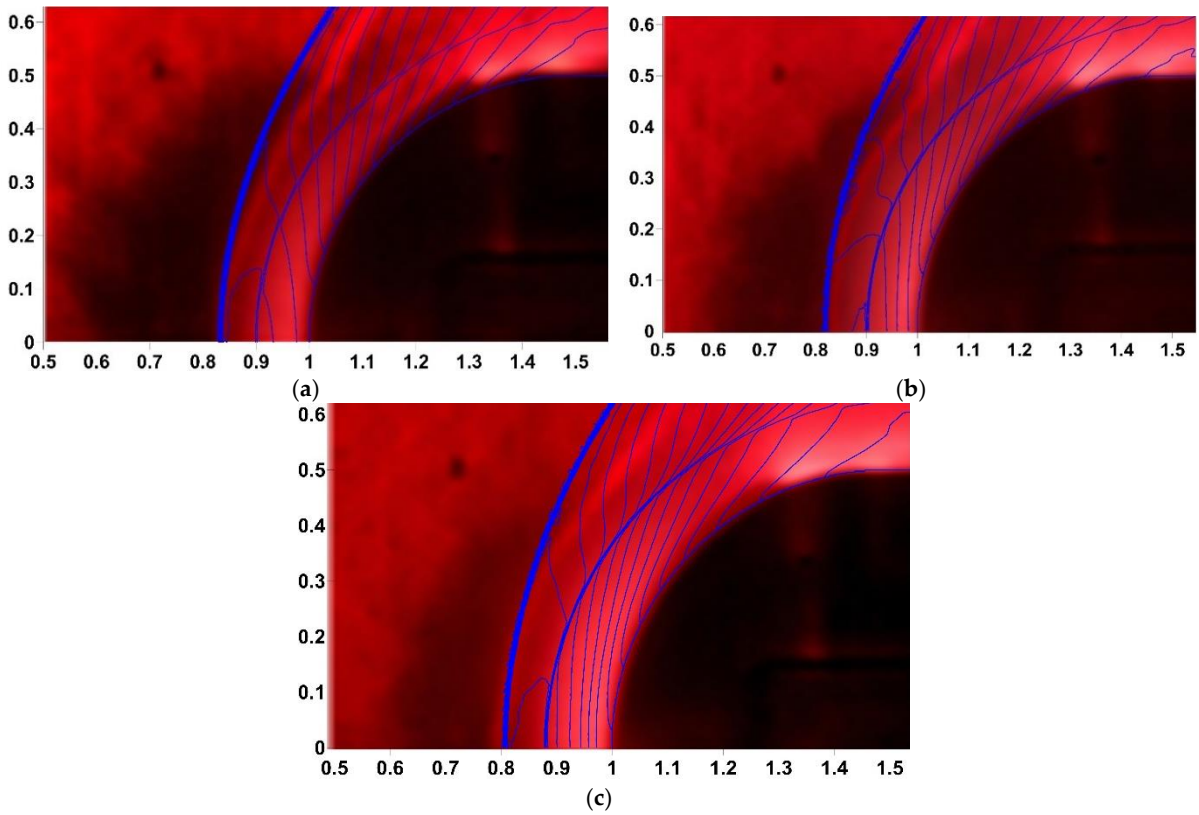

Figure 22. Comparison of the numerical flow patterns with the schlieren images of the near-surface discharge action in xenon; a) *I*=370 A, *P*=35 kW; b) *I*=670 A, *P*=68 kW; c) *I*=915 A, *P*=124 kW.

Table 3 shows a correspondence between the specific power produced by the discharge q, the discharge current I, and the value of the adiabatic index in the discharge zone γ_s. Here q_{dim} is the dimensional value of q. It is seen, that with the growth of the discharge current, the specific power increases; the adiabatic index γ_s remains practically the same, in the interval 1.25-1.258, with one oscillation occurs when γ_s =1.275; for large values of the discharge current the adiabatic index γ_s increases.

Table 3. Correspondence between the discharge current I, the specific power q, and the adiabatic index γ_s.

I, A	0	373	604	673	800	915
q	0	52	82.5	119.5	147.2	213.3
$q_{dim}\times10^{-6}$ kW/kg	0	36.312	57.610	83.447	102.790	148.947
γ_s	1.258	1.256	1.25	1.275	1.253	1.288

A correspondence between the discharge current I, discharge power P, the average density ϱ_a, temperature T_a, pressure p_a, in the plasma zone, the electron density n_e, the degree of ionization α, and the adiabatic index γ_s for Θ=1 (calculated using the theory of K. Burm et al. [24]) is presented in Table 4.

Table 4. Correspondence between the discharge current I, power P, the average parameters in the plasma zone, the electron density n_e, the degree of ionization α, and the adiabatic index γ_s for Θ=1 (calculated using the theory of K. Burm et al. [24]).

I, A	P, W	ϱ_a, kg/m3	T_a, K	p_a, P	n_e*10^{-22}	α	γ_s for Θ=1

 doi:10.20944/preprints202410.1285.v1

0	0	0.19180	7530.2	94900.9	1.65	0.01871	1.26
373	35099.2	0.17759	8507.3	95868.2	2.03	0.02486	1.262
604	54166.8	0.17275	9003.6	96546.7	2.70	0.03399	1.245
673	66345.3	0.146076	10905.1	96281.7	3.0	0.04467	1.269
800	86576.5	0.154749	10647.2	97396.8	3.57	0.05018	1.252
915	124693	0.125886	14064.2	98334.9	4.08	0.07049	1.295

It can be seen that with an increase in the discharge current and power, the average density decreases, and the pressure is weakly dependent on the discharge current. The plasma parameters, such as the electron density and the degree of ionization are increasing with the discharge current, and the adiabatic index for θ=1 is increasing overall, but experiences some oscillations (see, also, Part 5).

5. Comparison of the Results Obtained with the Dependences Defined by the Theory of K. Burm et al.

Figure 23 shows the dependences of the adiabatic index γ_s on the degree of nonequilibrium in the gas discharge zone, obtained according to the theory of K. Burm et al. [24] for the gas temperature and the average density calculated in numerical simulation when energy is supplied to the impact zone. For each value of the gas discharge current, the degree of ionization and gas temperature are determined and the dependence on θ is plotted. Calculations have shown that the corresponding values of γ_s obtained in numerical simulation are close to the values of the adiabatic index calculated according to the theory of K. Burm et al. at θ=1. This is quite understandable and once again confirms that the state of the plasma in the braking zone near the model is close to thermodynamic equilibrium at the steady flow mode.

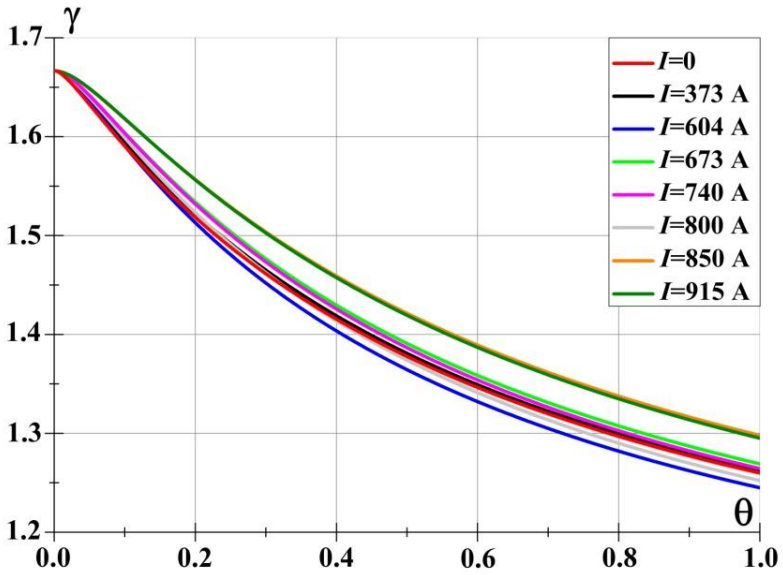

Figure 23. Dependence of the adiabatic index on the degree of nonequilibrium in the impact zone for different values of the discharge current.

In Figure 24, the same data are presented as dependences of the adiabatic index on the degree of plasma ionization in the impact zone at a fixed value of θ=1. The dashed vertical lines show the values of α for each value of the discharge current, and the horizontal lines show the corresponding values of the adiabatic index. From the curves in Figure 24 it can be concluded that by changing the

 doi:10.20944/preprints202410.1285.v1

plasma characteristics in the impact zone it is possible to change the value of the adiabatic index in a wide range of values, and therefore actively influence the process of supersonic flow around AD objects.

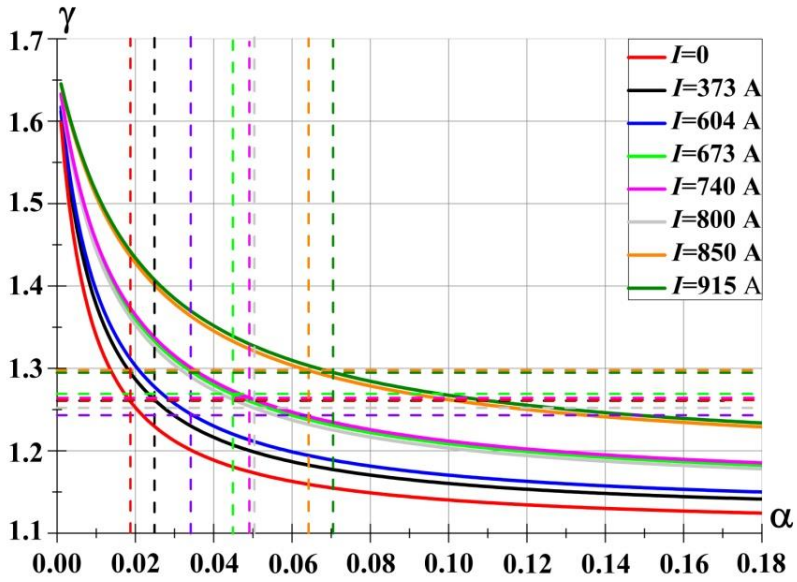

Figure 24. Dependence of the adiabatic index on the degree of ionization in the impact zone for different values of the discharge current at thermodynamic equilibrium.

In addition, it is seen from these dependences that an increase in the ionization degree leads to a decrease in the adiabatic index (at a fixed current and gas temperature), and an increase in the gas temperature (at a fixed ionization degree) leads to its increase. It is also evident that the curves in Figure 24 are divided into three groups of curves: 1 - at the discharge currents of 0-600 A; 2 - at the currents of 600-800 A and 3 - at the currents greater than 800 A, the curves in the groups differ slightly from each other. Such a division leads to non-monotonicity of the dependence of the adiabatic index on the discharge current and the supplied power and, as a result, to non-monotonicity of the dependence of the value of the relative stand-off distance (see Figure 21).

A comparison of the dependences of the adiabatic index on the value of the gas-discharge current and on the specific power of the energy supplied to the impact plasma zone obtained in numerical modeling and calculated according to the theory of K. Burm et al. is shown in Figure 25. The non-monotonic nature of the dependencies shows a significant sensitivity of the adiabatic index γ_s to the plasma characteristics. In the range of currents 1 (of 0-600 A), the adiabatic index γ_s changes slightly, changes in the degree of ionization and gas temperature are not enough for significant changes in the adiabatic index γ_s. In the range 2 (of 600-800 A), the influence of plasma characteristics is strong, γ_s can both increase and decrease. In the range 3 (the current is greater than 800 A), γ_s begins to be determined by the gas temperature, which leads to its growth. Thus, a good agreement of the numerical results and the data calculated according to theory of K. Burm et al. was obtained. In addition, the non-monotonic dependence of the adiabatic index γ_s on the discharge current and the specific power in both calculations was shown, as well.

 doi:10.20944/preprints202410.1285.v1

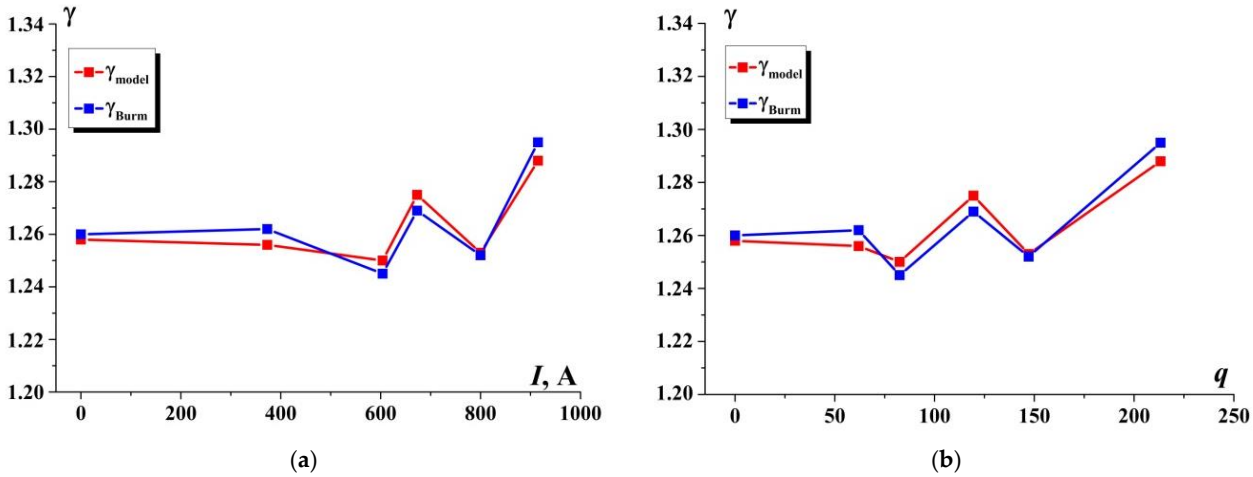

Figure 25. Comparison of the values of the adiabatic index γ_s obtained in numerical simulation and calculated using the theory of K. Burm et al. [24] in the dependence on the gas discharge current (a) and the specific power (b).

6. Conclusions

The experimental and numerical results of the study of the influence of the near-surface plasma zone of the AD body, formed during the organization of a glow gas discharge in xenon, on the position of the stationary bow shock wave are presented. The fields of the flow parameters were examined for different values of the discharge specific power q and adiabatic index in the plasma region γ_s. Good agreement was found when comparing the numerical and experimental values of the relative stand-off distance of the bow shock wave.

The obtained new results are as follows:

- It was obtained that when the discharge power is in the interval $0<P<5.42\times10^5$W and the discharge current is in the interval $0<I<600$A, the dependence of the relative stand-off on the discharge power is close to linear. Besides, the oscillation of the relative stand-off distance was obtained at 1.25×10^5W$<P<8.66\times10^5$W and 600A$<I<$800A. This oscillation is associated with a strong dependence of the adiabatic index γ_s on the degree of ionization in this current range, which can lead to both its increase and decrease.
- The comparison is presented for the results obtained with taking into account the initial ionization ahead of the model and without it. It was concluded that taking into account the primary ionization ahead of the body is important both for small currents (since for these values there is a noticeable difference in the values of γ_s) and for large currents, for which a large difference in the estimates of the necessary discharge specific power was obtained.
- A correspondence between the specific power q produced by the discharge, the discharge current I, and the value of the adiabatic index in the discharge zone γ_s. was analyzed. It is shown that the adiabatic index with the power supplied to the impact zone in the range of 30-120 kW can both increase and decrease in the range of 1.25-1.288. It was obtained that with the growth of the discharge current, the specific power increases, and γ_s tends to increase.
- Based on the experimental results, the simulations yielded average values of density, pressure, temperature, electron density, degree of ionization, and degree of non-equilibrium for the monoatomic xenon plasma in the steady flow regime. It was shown that with an increase in the discharge current and power, the average density in the action zone decreases, the temperature is increasing, and the pressure is weakly dependent on the discharge current. The plasma

 doi:10.20944/preprints202410.1285.v1

parameters, such as the electron density and the degree of ionization were shown to increase with the discharge current.

- A strong dependence of the adiabatic index γ_s on the degree of ionization and the degree of nonequilibrium was shown experimentally and numerically, which was in agreement with the theory of K. Burm et al. It was shown that the corresponding values of γ_s obtained in numerical simulation are close to the values of adiabatic index calculated according to the theory of K. Burm et al. at thermodynamic equilibrium.
- It was found that, depending on the range of the gas-discharge current, it is possible to distinguish different degrees of influence of plasma characteristics on the value of γ_s: weak at the currents of 0-600 A, strong at the currents of 600-800 A, when γ_s can both increase and decrease with a small change in the degree of ionization, and thermal in the range >800 A, where γ_s is determined mainly by the gas temperature.
- It was shown that the steady position of the bow shock wave is significantly affected by both the specific discharge power q and the gas adiabatic index γ_s in the discharge plasma zone, which is determined by the characteristics of the plasma zone, namely the average density, pressure, temperature, as well as the degree of ionization and the degree of nonequilibrium.

Thus, this study demonstrates the feasibility of controlling both the steady state position of the bow shock wave and the characteristics of an AD body in xenon by creating a volumetric, monoatomic xenon plasma region in front of its entire cylindrical frontal surface. These findings have potential for the development of control systems for high-speed civil aircraft.

Author Contributions: Data curation, Olga Azarova and Tatiana Lapushkina; Formal analysis, Olga Azarova, Tatiana Lapushkina and Oleg Kravchenko; Investigation, Olga Azarova and Tatiana Lapushkina; Methodology, Olga Azarova and Tatiana Lapushkina; Software, Olga Azarova; Supervision, Olga Azarova; Validation, Olga Azarova; Visualization, Olga Azarova and Tatiana Lapushkina; Writing – original draft, Olga Azarova, Tatiana Lapushkina and Oleg Kravchenko; Writing – review & editing, Olga Azarova and Oleg Kravchenko.

Funding: The study was supported by the Ministry of Science and Higher Education of the Russian Federation, project No. 075-15-2024-544.

Conflicts of Interest: The authors declare no conflict of interest.

Nomenclature

Parameters

D, m; R, m	diameter and radius of an aerodynamic body
d, m	bow shock wave stand-off distance from the body
d_0, m	bow shock wave stand-off distance from the body at the absence of energy deposition
F, N	drag force of the body's front surface
F_0, N	drag force of the body's front surface at the absence of energy deposition
h_x, h_y	space steps
I, A	discharge current
J, A/m^3	gas discharge current density
M	Mach number
M_1	Shock wave Mach number in the shock tube
n_e, m^{-3}	electron concentration
p, P, ρ, kgm^{-3}, T, K	pressure, density, and temperature of the gas
P, W	discharge power
q, kW/kg	specific power
Re, Pr	the Reynolds number and the Prandtl number
$\boldsymbol{U}$, m/s	vector of the flow velocity, $\boldsymbol{U}=(u,v)$

 doi:10.20944/preprints202410.1285.v1

U_{pl}, V	voltage across the discharge gap
X_{bsw}, m	coordinate of the bow shock wave
α	degree of ionization
γ	adiabatic index (ratio of specific heats, isentropic exponent)
γ_s	adiabatic index in the discharge created plasma region
θ	degree of nonequilibrium
σ, S/cm	effective plasma conductivity

Indices

t	parameters at the central point of the semi-cylinder
a	average flow characteristics in the discharge created plasma region
n	normalizing parameters
∞	freestream parameters
cr	parameters in the critical section of the nozzle
e	parameters of electrons
h	parameters of heavy particles

Abbreviations

AD	aerodynamic
MHD	magnetohydrodynamic
MW	microwave

References

1. Knight, D.D. *Energy Deposition for High-Speed Flow Control*; Cambridge University Press: Cambridge, UK, 2019; 450p.
2. Knight, D. Survey of aerodynamic drag reduction at high speed by energy deposition. *J. Propuls. Power* **2008**, *24*, 1153–1167.
3. Ahmed, M.Y.M.; Qin, N. Forebody shock control devices for drag and aero-heating reduction: A comprehensive survey with a practical perspective. Prog. Aerosp. Sci. **2020**, *112*, 100585.
4. Rashid, S.; Nawaz, F.; Maqsood, A.; Salamat, S.; Riaz, R. Review of wave drag reduction techniques: Advances in active, passive, and hybrid flow control. *Proc. Inst. Mech. Eng. Part G J. Aerosp. Eng.* **2022**, *12*, 2851–2884.
5. Leonov, S.B.; Adamovich, I.V.; Soloviev, V.R. Dynamics of near-surface electric discharges and mechanisms of their interaction with the airflow. *Plasma Sources Sci. Technol.* **2016**, *25*, 063001.
6. Leonov, S.B. Review of plasma-based methods for high-speed flow control. In Proceedings of the Sixth International Conference on Fluid Mechanics AIP Conference Proceedings, Guangzhou, China, 30 June–3 July 2011; pp. 498–502.
7. Znamenskaya, I.A. Methods for panoramic visualization and digital analysis of thermophysical flow fields. A review. *Sci. Vis.* **2021**, *13*, 125–158.
8. Georgievsky, P.Y.; Levin, V.A Control of the flow past bodies using localized energy addition to the supersonic oncoming flow. *Fluid Dyn*. **2003**, *38*, 794–805.
9. Artem'ev, V.I.; Bergel'son, V.I.; Nemchinov, I.V.; Orlova, T.I.; Smirnov, V.A.; Hazins, V.M. Changing the regime of supersonic streamlining obstacles via raising the thin channel of low density. *Izv. Akad. Nauk SSSR Meh. Židk. Gaza* **1989**, *5*, 146–151. (In Russian)
10. Riggins, D.; Nelson, H.F.; Johnson, E. Blunt-body wave drag reduction using focused energy deposition. *AIAA J.* **1999**, *37*, 460–467.
11. Kolesnichenko, Y.; Brovkin, V.; Azarova, O.; Grudnitsky, V.; Lashkov, V.; Mashek, I. Microwave energy release regimes for drag reduction in supersonic flows. *40th AIAA Aerospace Sciences Meeting & Exhibit*, AIAA Paper No. 2002-0353, **2002**.
12. Tretyakov, P.K.; Fomin, V.M.; Yakovlev, V.I. New principles of control of aerophysical processes—Research development. In Proceedings of the International Conference on the Methods of Aerophysical Research, Novosibirsk, Russia, 29 June–3 July 1996; p. 210.
13. Bityurin, V.A.; Klimov, A.I.; Leonov, S.B.; Potebnya, V.G. On interaction of longitudinal pulse discharge with bow shock. In Proceedings of the Workshop "Perspectives of MHD and Plasma Technologies in Aerospace Applications", IVTAN, Moscow, Russia, 24–25 March 1999; p. 114.

 doi:10.20944/preprints202410.1285.v1

14. Bityurin, V.A.; Klimov, A.I.; Leonov, S.B.; Lutsky A. E.; Van Wie, D.; Brovkin, V. G.; Kolesnichenko, Yu. F. Effect of heterogeneous discharge plasma on shock wave structure and propagation. Proceedings of the 3rd Weakly Ionized Gases Workshop, Norfolk, VA, USA, 1–5 November 1999; AIAA Paper 1999-4940.
15. Benard, N.; Moreau, E. Electrical and mechanical characteristics of surface AC dielectric barrier discharge plasma actuators applied to airflow control. *Experiments in Fluids* **2014**, *55*.
16. Lapushkina, T.A.; Erofeev, A.V. Supersonic flow control via plasma, electric and magnetic impacts. Aerosp. Sci. Technol. **2017**, *69*, 313–320.
17. Lapushkina, T.A.; Vasil'eva, R.V.; Erofeev, A.V.; Ponyaev, S.A.; Bobashev, S.V. Ionization Kinetics in a Supersonic Xenon Plasma Flow Entering Electric Field. *Technical Physics Letters* **2004**, *30*, 724–726.
18. Bobashev, S.; Mende, N.; Sakharov, V.; Van Wie, D. MHD Control of the Separation Phenomenon in a Supersonic Xenon Plasma Flow. *41st Aerospace Sciences Meeting and Exhibit,* AIAA Paper No. 2003-168, **2003**.
19. Bobashev, S.; Mende, N.; Sakharov, V.; Van Wie, D. MHD Control of the Separation Phenomenon in a Supersonic Xenon Plasma Flow II. *42nd AIAA Aerospace Sciences Meeting and Exhibit,* AIAA Paper No. 2004-0515, **2004**.
20. Zhao, X.; Xiang, X.; Yu, J.; Shen, Q. An experiment investigation on shock-induced turbulent boundary layer separation flow-field. In Proceedings of 54th AIAA Aerospace Sciences Meeting, San Diego, California, USA, **2016**.
21. Yan, H.; Liu, F.; Xu, J.; Xue, Y. Study of oblique shock wave control by surface arc discharge plasma. *AIAA Journal* **2017**, *56*, 532–541.
22. Tang, B.; Guo, S.; Hua, L. Experimental study on high-energy surface arc plasma excitation control of cylindrical detached shock wave. *Contributions to Plasma Physics* **2020**, *61*.
23. Azarova, O.A.; Erofeev, A.V.; Lapushkina, T.A. A comparison of plasma and thermal effects upon supersonic flow past aerodynamic bodies. *Tech. Phys. Lett.* **2017**, *43*, 405–408.
24. Burm, K.T.A.L.; Goedheer, W.J.; Schram, D.C. The isentropic exponent in plasmas. *Physics of Plasmas* **1999**, *6*, 2622–2627.
25. Lago, V.; Joussot, R.; Parisse, J. Influence of the ionization rate of a plasma discharge applied to the modification of a supersonic low reynolds number flow field around a cylinder. *Journal of Physics D Applied Physics* **2014**, *47*, 125202.
26. Azarova, O.A.; Lapushkina, T.A.; Shustrov, Y.A. Near-surface gas discharge effect on a steady bow shock wave position in a supersonic flow past a cylindrically blunted body in the air. *Phys. Fluids* **2022**, *34*, 066117.
27. Raizer, Yu. P. *Gas Discharge Physics* (Springer, Berlin, 1991).
28. Roache, P. J. *Computational Fluid Dynamics* (Mir, Moscow, 1980).
29. Azarova, O. A. Complex conservative difference schemes for computing supersonic flows past simple aerodynamic forms, *Comput. Math. Math. Phys.* **2015**, 55(12), 2025-2049.